

Organic Electrochemical Transistor, Understanding and Modifying for Sensing Applications

by

Salva Salmani-Rezaie

A thesis submitted in partial fulfillment of the requirements for the degree of

Master of Science

in

Materials Engineering

Department of Chemical and Materials Engineering
University of Alberta

© Salva Salmani-Rezaie, 2016

Abstract

The field of conducting polymers and mainly organic electrochemical transistors (OECT) have been investigated for bioelectronics applications. Advantages such as conformability, high quality electrical contact, ease of fabrication and biocompatibility made OECTs a great potential of future bio diagnostic tools. Also, PEDOT: PSS conjugate polymer have emerged as an attractive polymer for a various application in the last years. In this study the working mechanism of OECT based on PEDOT: PSS has been studied to obtain parameters for designing biosensors. OECTs based on flexible substrate have been fabricated with high ON/OFF current ratio (2×10^3). Using gate current transient as a response to gate voltage pulsing at different gate voltages, the total amount of charge and capacitance per unit area has been calculated. Preliminary result showed the specific capacitance value to be 57 F/cm^3 . Effect of channel geometry on device performance has been studied and it has been found that devices with high w/l ratio has higher transconductance. Channel thickness also has major role in OECTs transconductance. By decreasing channel thickness, transconductance decreases however it reaches its maximum at lower gate voltages, indicating lower operating voltages for higher sensitivity for biosensing.

Previous studies demonstrated application of PEDOT: PSS as an active material of depletion mode organic electrochemical transistor (OECT). In this work, we used over oxidized PEDOT: PSS film as a channel material of OECT and observed accumulation behavior. We study the structure of over-oxidized PEDOT: PSS and notice PEDOT degradation during over-oxidation process, while PSS remains intact. As a result, throughout this reaction, the electronic conductivity of PEDOT chain decrease dramatically. However,

the ionic conductivity occurs primarily in the excess PSS and is independent of the oxidation state of PEDOT. This initiates a device which switches from depletion mode to accumulation mode by a simple oxidation process of hypochlorite treatment. In summary this work contributes to the better understating of OECTs and channel structure on working principle of OECTs to design future less invasive neuro-probes.

Acknowledgment

I would like to express my sincere appreciation to my supervisors Dr. Carlo Montemagno and Dr. Manisha Gupta for their support and guidance throughout my program. They continually conveyed the spirit of adventures and showed there is no limit to ingenuity and no boundary on what science can explore. I would also like to extend my appreciation to my committee member, Dr. Chung for his insightful comments.

I would also like to extend my gratitude to Susan Kuzmak, Jeff Germain and my friends at ingenuity lab to make this journey easier and fun. I would like to thank university of Alberta's Nanofab staff specially Les Schowalter, Scott Munro, Dimitre Karpuzov and Shihong Xu whom helped with developing the fabrication and characterization steps. In addition, a huge thank you to NINT's clean room members, Mike O'toole, Tim Patrie and Rob Indoe. They made fabrication so fun and they never told no for what I have asked for.

Words cannot describe how much I am grateful to my always supportive caring lovely family. I love you my dearest Baba Ali, Maman Akhtar, Saber and Sama. No matter how far we are, your love, supports, prayers and advices are with me.

Last but not least I want to thank my great husband Kaveh. My favorite scientist, thank you for being such a patient teacher and great supervisor at home. Azizam thank you to always be with me and to encourage me to reach the stars.

Table of content

<i>1 Introduction.....</i>	<i>1</i>
<i>1-1 Background.....</i>	<i>1</i>
<i>1-2 Conducting polymers</i>	<i>2</i>
<i>1-2-1 Orbitals and bonds.....</i>	<i>3</i>
<i>1-2-2 Electronic structure of conducting polymers.....</i>	<i>6</i>
<i>1-2-3 Charge carriers and Charge transport in conducting polymers</i>	<i>7</i>
<i>1-2-4 Poly (3 4-ethylenedioxythiophene)-Poly (styrene sulfonate).....</i>	<i>10</i>
<i>1-3 Organic transistors</i>	<i>11</i>
<i>1-3-1 Organic Field Effect Transistor</i>	<i>12</i>
<i>1-3-2 Organic Electro Chemical Transistor</i>	<i>14</i>
<i>1-3-3 OECT based Sensors</i>	<i>16</i>
<i>1-4 Objective of this work</i>	<i>18</i>
<i>1-5 Outline of thesis</i>	<i>19</i>
 <i>2 Experimental procedure</i>	 <i>21</i>
<i>2-1 OECT device fabrication</i>	<i>21</i>
<i>2-2 Electrical measurement</i>	<i>26</i>
<i>2-3 PEDOT: PSS film characterization.....</i>	<i>27</i>

2-3-1 Ellipsometry	27
2-3-2 Four-point probe.....	27
2-3-3 XPS/UPS	28
2-3-4 Raman spectroscopy.....	29
<i>3- Organic Electrochemical Transistor, characteristics and operation mechanism.</i>	30
3-1 Introduction	30
3-2 Results and discussion	32
3-2-1 PEDOT: PSS film characterization	32
3-2-2 OECT device operation	35
3-2-3 OECT operation model.....	47
3-3 Conclusion	52
<i>4 -Oxidation Effect of PEDOT: PSS Channel Material on Combined Depletion and Accumulation Regime OECT.....</i>	54
4-1 Introduction	54
4-2 Results and discussion	56
4-2-1 effect of over oxidation on PEDOT: PSS chemical structure change	56
4-2-2 Effect of over-oxidation on PEDOT: PSS electronic structure change.....	61
4-3 Conclusion	68
<i>5 Conclusion and future work.....</i>	69
<i>Bibliography.....</i>	72

<i>Appendix A</i>	79
<i>A-1 OECT fabrication steps</i>	79
<i>A-2 OECT fabrication based on sacrificial layer of Parylene</i>	81
<i>Appendix B</i>	84

List of figures

Figure 1-1 Schematic of formation of bonding and antibonding orbitals by overlap of two p orbital of carbon atom	4
Figure 1-2 The energy level splitting of two bounded dimer and formation of band gap	5
Figure 1-3 hybrid orbitals: from left to right sp, sp ² , sp ³ orbitals	5
Figure 1-4 chemical structure (left) and σ bounded orbitals	6
Figure 1-5 Chemical structure and σ/π bonding of trans polyacetylene	7
Figure 1-6 schematic of soliton formation in trans polyacetylene and associated energy level of neutral, positive and negative soliton.....	8
Figure 1-7 Schematic of neutral aromatic state, positive polaron and positive bipolaron and their associated band diagram	9
Figure 1-8 chemical structure of PEDOT: PSS hole (positive polaron) on PEDOT balance by SO ₃ ⁻ ion of PSS chain.....	11
Fig 1-9 a) formation of EDL at gate/electrolyte and channel/electrolyte surface b) ion (above) and potential (below) distribution in Helmholtz and diffusion layer.....	14
Fig 1-10 Schematic of OECT behavior a) OECT components. b) OECT without gate voltage applied. c) OECT with gate voltage (V _G).....	15
Figure 2-1 (a) Parylene deposition (b)Source, drain and contact pad deposition (c)Parylene deposition to insulate electrodes (d) channel and gate opening (RIE) (e) channel and gate coating (f)PEDOT: PSS patterning (The schematic is not to scale)	21
Figure 2-2 Deposition process of parylene-C	22
Figure 2-3 Designed photomask layout for different steps of optical lithography	23
Figure 2-4 confocal microscope image of OECT	26
Figure 3-1 (a) experimental \square and $\square\square\square$ data and the assigned optical model (red line) and (b) uniaxial anisotropic of refraction and extinction coefficients	33
Figure 3-2 PEDOT: PSS film thickness at different spin coating rates	34
Figure 3-3 change in resistance and conductivity of PEDOT: PSS film by its thickness.....	35

Figure 3-4 schematic layout of device and channel geometry and output characteristics of the device with dimensions of $w=20\mu\text{m}$, $l=40\mu\text{m}$ and $d=260\text{nm}$. V_G changing between 0 (top curve) to 0.7 V (bottom curve)36

Figure 3-5 a) transfer curve for V_D changing from 0 (bottom curve) to -0.6V (top curve) and OECT transconductance for V_D of -0.6v (top curve) and -0.1V (bottom curve) for the device with dimension of $w=20\mu\text{m}$, $l=40\mu\text{m}$ and $d=260\text{nm}$38

Figure 3-6 transfer and transconductance curve of the OECT for the device with dimension of $w=20\mu\text{m}$, $l=20\mu\text{m}$ and $d=260\text{nm}$ at $V_D=-0.6\text{V}$ 39

Figure 3-7 transconductance as a function of device geometry all measurements have been done at $V_D= -0.6\text{V}$ ($d=260\text{nm}$).....40

Figure 3-8 transfer characteristics with indication of ON/OFF current ratio and threshold voltage for the device with dimension of $w=20\mu\text{m}$, $l=40\mu\text{m}$ and $d=260\text{nm}$ at $V_D=-0.6\text{V}$..42

Figure 3-9 crumpled device and its output characteristics before being peeled and after being peeled and crumpled ($w=10\mu\text{m}$, $l=30\mu\text{m}$, $d=260\text{nm}$)43

Figure 3-10 a) output characteristics of the device. V_G changing between 0 (top curve) to 0.6 V (bottom curve) b) transfer curve for V_D changing from 0 (bottom curve) to -0.6V (top curve) c) and OECT transconductance for V_D of -0.6v (top curve) and -0.1V (bottom curve) d) transfer characteristics with indication of ON/OFF current ratio and threshold voltage e) transconductance as a function of device geometry for V_D of -0.6v for the device with dimension of $w=20\mu\text{m}$, $l=40\mu\text{m}$ and $d=170\text{nm}$ at $V_D=-0.6\text{V}$ 45

Figure 3-11(a)schematic of device measurement, (b) Gate current transient from an OECT with dimensions of $w=10\mu\text{m}$, $l=40\mu\text{m}$ and $d=260\text{nm}$ and the inset is an image of pulse voltage applied to the gate.....48

Figure 3-12 injected charge as a function of gate voltage for OECT of $w=10\mu\text{m}$, $l=40\mu\text{m}$ and $d=260\text{nm}$49

Figure 3-13 output characteristics of the device. V_g changing between 0 (top curve) to 0.6 V (bottom curve) symbols shows the saturation region b) transfer characteristics with indication of ON/OFF current ratio and threshold voltage for the device c) points indication of I_D based on OECT model and real data with dimension of $w=10\mu\text{m}$, $l=40\mu\text{m}$ and $d=260\text{nm}$51

Fig A- 1) Parylene deposition (a) Source, drain and contact pad deposition (b) Parylene deposition to insulate electrodes(c)) Sacrificial parylene deposition (d) channel and gate opening (RIE) and PEDOT: PSS coating (e) Sacrificial layer removing and PEDOT: PSS baking (f).....82

Figure A-2 Optical microscope image of OECTs fabricated by sacrificial layer of Parylene83

Figure B-1output characteristics of the device with dimensions of $w=20\mu\text{m}$, $l=50\mu\text{m}$ and $d=170\text{nm}$. V_G changing between 0 to 0.5 V (right OECT based on pristine PEDOT: PSS and depletion mode device and left OECT based on over-oxidized PEDOT: PSS and accumulation device)84

Figure B-2 output characteristics of the device with dimensions of $w=20\mu\text{m}$, $l=40\mu\text{m}$ and $d=260\text{nm}$. (right OECT based on pristine PEDOT: PSS and depletion mode device and left OECT based on over-oxidized PEDOT: PSS and accumulation device)85

Figure B-3 output characteristics of the device with dimensions of $w=20\mu\text{m}$, $l=5\mu\text{m}$ and $d=260\text{nm}$. (right OECT based on pristine PEDOT: PSS and depletion mode device and left OECT based on over-oxidized PEDOT: PSS and accumulation device)85

List of tables

1. Table 3-1 OECT characteristics for two different channel thickness and same length and width ($w=20\mu\text{m}$ and $l=40\mu\text{m}$).....47
2. Table4-1 energy level of pristine and oxidized PEDOT :PSS sample studied by UPS63

Abbreviation

Highest Occupied Molecular Orbital (HOMO)

Lowest Unoccupied Molecular Orbital (LUMO).

Poly (3 4-EthyleneDiOxyThiophene)-Poly (Styrene Sulfonate) (PEDOT: PSS)

(3-glycidyoxypropyl) trimethoxysilane (GOPS)

DodecylBenzene Sulfonic Acid (DBSA)

Organic Field Effect Transistor (OFET)

Organic Electro Chemical Transistor (OECT)

Electrical Double Layer (EDL)

Reactive Ion Etching (RIE)

Full Width Half Maximum (FWHM)

X-ray Photoelectron Spectroscopy (XPS)

Ultraviolet Photoelectron Spectroscopy (UPS)

1 Introduction

1-1 Background

Polymers are macromolecules that consist of many elementary units which are covalently bonded together. Natural polymers were existing long before the concept of polymer has even been introduced. DNA, protein and cellulose are all examples of natural polymers. The concept of macromolecules and polymers introduced by study of Hermann Staudinger which led to the Chemistry Nobel prize at 1953. However, this was just beginning of polymer era and today plastic synthetic polymers exist in many aspects of everyday life. In our days, one can tailor chemical, mechanical and optical properties of polymer by changing chemical structure and composition of monomers.

Traditionally polymers have been known and used as insulator material. However, investigations of Alan J. Heeger, Alan G. MacDiarmid and Hideki Shirakawa, launched the concept of conductive polymer. In 1977, they demonstrated that the conductivity of polyacetylene increases several orders of magnitude by exposing it to iodine vapor. This discovery was foundation of chemistry Nobel Prize of year 2000 as well as new class of electronics coined as organic electronics. Nowadays, organic electronics have been studied extensively in the field of light emitting diodes^{1,2}, solar cells^{3,4}, thin film transistors^{5,6} and thermoelectric devices^{7,8}. Although organic semiconductors cannot compete with inorganic materials in terms of charge transport and stability, they have other advantages. Ease of fabrication, cheap fabrication cost, large area- high volume fabrication,

biocompatibility and compatibility with flexible substrates are some of the organic electronics properties that make them appealing. Beside these characteristics, being porous gives organic semiconductors the ability to transport ions beside electrons. This makes them very good candidate for bio-sensing applications where biological events, change the ion concentration and can therefore change chemical and electronic structure of organic based sensors. Development of organic and flexible electronic biosensors can open a way for early diagnoses and treatment of brain disorders.

Central nervous system disorders affect brain, spinal cord and nerves that connect them. There are around one billion people who are suffering from more than 600 mental diseases like Depression, Schizophrenia, Alzheimer, Parkinson, Epilepsy and MS. Most of these diseases are progressive in nature starting from simple symptom and leading to functional limitation and at times fatal. Basic study of brain's chemical and its dynamic voltage provides the opportunity for early diagnose and control of these disorders.

1-2 Conducting polymers

Polymers are carbon based macromolecules composed of several (poly) repeated units (monomer). Conventional polymers are generally known to be insulator. However, discovery of conducting polymers in 1977 by Alan J. Heeger, Alan G. MacDiarmid and Hideki Shirakawa^{9,10} changed its function from plastic insulator material to electroactive material in organic and bio-electronic devices. In this chapter, molecular bonds between

atoms, electronic and chemical structure of conducting polymers and associated electronic conductivity will be described.

1-2-1 Orbitals and bonds

Atom is basic building block of matter which is consist of positively charged nucleus surrounded by cloud of negatively charged electrons. Electrons do not randomly occupy the region around nucleus and their position in atom are described by quantum mechanics wave function ($\Psi (r,t)$). According to quantum mechanics, electrons are more probable to be found at wave functions which are solution of Schrödinger equation. These wave functions are called atomic orbitals and based on their unique quantum numbers, they have specific energy and shape. Principle quantum number, n , determines the atomic shell (labeled by K, L, M, N, etc.) and orbital angular momentum, l and m , defines the atomic subshell (labeled by s, p, d, f, etc.). based on Pauli's exclusion principle, only two electrons with different spin state can occupy same orbital ^{11,12}.

When two atoms come close to each other, their valance electrons interact with each other and their atomic wave function overlap. As the valence electrons in the combined system are shared and attracted by two nuclei, they are described by new wave function that is called molecular orbital. Interfering of two atomic orbitals could be in phase, resulting into bonding orbitals and stable molecule or could be out of phase, resulting into antibonding orbitals with higher energy compared to bonding orbital. As a result, by formation of bonding and antibonding orbitals, there is splitting of atomic energy level into

two molecular level in an energy diagram. Electrons first fill the orbitals with lower energy level ^{11,12}. Figure 1-1, is a schematic of formation bonding (π) and antibonding (π^*) orbitals when two carbon atom brought close to each other. The in phase bonding results into energy level lower than original p orbitals and out of phase bonding cause an increase in energy of orbitals.

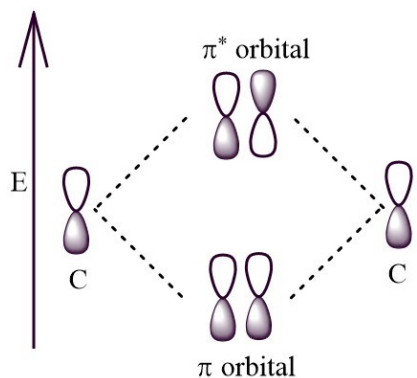


Figure 1-1 Schematic of formation of bonding and antibonding orbitals by overlap of two p orbital of carbon atom

When multiple atoms approach each other, the energy difference between orbitals becomes small, as a result, separated energy levels, form energy band. The highest energy level that is occupied with electron is called Highest Occupied Molecular Orbital (HOMO) and the lowest energy level is called Lowest Unoccupied Molecular Orbital (LUMO). The energy difference between the HOMO and LUMO is called band gap. Figure 1-2 represents the energy level splitting. When two dimer bound together, four different bonding and antibonding orbitals form. By increasing the number of dimers, the splitting of HOMO and LUMO continues and energy bands form. Molecular bonding is either symmetrical with

respect to inter-nuclear axis or asymmetrical which are labeled by σ (sigma) or π (Pi) respectively.

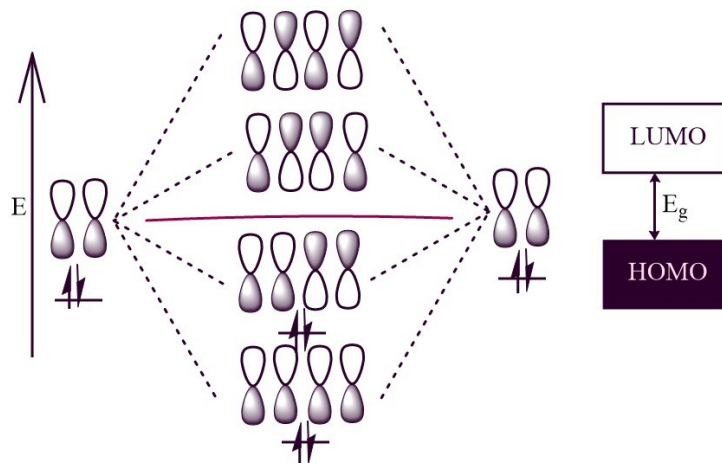


Figure 1-2 The energy level splitting of two bounded dimer and formation of band gap

Polymers are mainly formed from carbon backbone. Carbon has four electrons in the valence orbital by configuration of $2s^2 2p_x^1 2p_y^1$ in its ground state. While next to other element, carbon forms excited state by promoting one of the electrons from s orbital to one empty state of p orbital to maximize the number of bonds and minimize the system energy. The electron in s orbital can be hybridized with one, two or three electron of p orbital and forms two sp , three sp^2 or four sp^3 hybrid orbital. These hybrid orbitals are shown in figure 1-3.

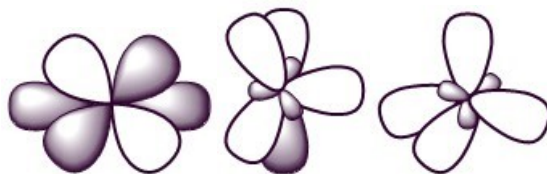


Figure 1-3 hybrid orbitals: from left to right sp , sp^2 , sp^3 orbitals

In regular insulator polymers, all electrons are in strong covalent bond with neighboring atom. Simple example of such polymer is polyethylene where each carbon is sp^3 hybridized. In this case all valence electrons are involved in strong σ bond with adjacent hydrogen and carbon atom. Figure 1-4 shows chemical structure and σ bonds between sp^3 hybrid orbitals. Unlike insulator polymers there is another class of semiconducting/conducting polymers called conjugated polymers, where all electrons are not bounded through σ bonding^{13,14}.

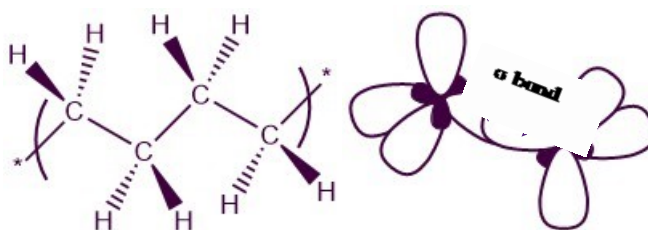


Figure 1-4 chemical structure (left) and σ bonded orbitals

1-2-2 Electronic structure of conducting polymers

Conjugated polymers are a class of polymers which have the ability to conduct electrical/ionic charge mainly due to π -conjugation in their structure. In conjugate polymers, each carbon atom forms three sp^2 hybridized state and three σ bond. The remaining valence electrons in the p_z orbitals of neighboring carbons overlap with each other and form delocalized π orbitals and π bonds. Electrons in π orbital are delocalized over polymer chain and do not belong to one single bond. By assuming equal bond length

in polymer chain, the bonds in conjugated chains leads to half-filled energy band like metals with no gap between HOMO and LUMO. However, based on Peierls instability theorem, this configuration (1-D metal) is not energetically favorable. Hence the polymer chain will undergo structure distortion and opens band gap by forming alternating short double bond and long single bond. Trans-polyacetylene is the simplest conjugated polymer. Chemical structure and bonding of polyacetylene is shown in Figure 1-5. Presence of π bond between p orbitals beside σ bond of sp^2 orbitals makes polymer conducting^{15,16}.

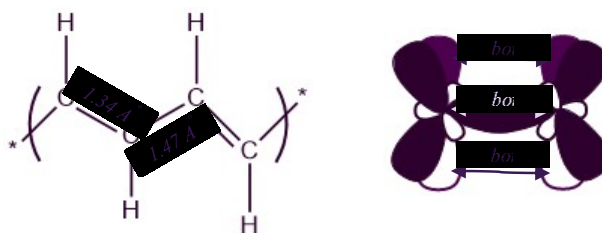


Figure 1-5 Chemical structure and σ/π bonding of trans polyacetylene

1-2-3 Charge carriers and Charge transport in conducting polymers

In conventional semiconductors, charge carriers are formed through addition or removal of electrons. In these materials electrons and holes (charge carriers) are delocalized in valance and conduction band and can move easily in crystal structure. Unlike inorganic semiconductors, in case of organic semiconductors electrons and holes will not be generated in HOMO or LUMO and defects are main charge carriers in conducting polymers. Charge carriers in conducting polymers are quasi-particles (soliton or polaron/bipolaron) which are formed by local molecular distortion of polymer chain.

Some polymers have a degenerate ground state, which means polymer can have two different conformations with same energy. In these conjugated polymers, the location of single and double bond can be changed without any change in energy of the system. As these bonds have same length and energy, they can be found on the same polymer chain with equal probability. In polymers with degenerate ground state and odd number of carbons, the unpaired π -electron locates between phase kink of single/double bond alternation. The interface between two phase is not clear and is extended along few units. The unpaired electron and bond distortion between two phase is called soliton. The neutral soliton, consists of unpaired electron and has spin of $\frac{1}{2}$. Neutral soliton can lose an electron and become positive soliton or gain one electron and become negative soliton. Both positive and negative solitons are spinless. The presence of soliton forms localized electronic level in the band gap and is charge carrier in degenerate conjugated polymers¹⁵⁻¹⁸. Schematic illustration of Neutral, negative and positive soliton in trans polyacetylene is shown in figure 1-6.

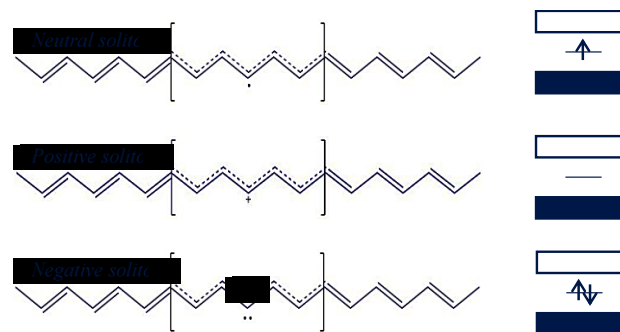


Figure 1-6 schematic of soliton formation in trans polyacetylene and associated energy level of neutral, positive and negative soliton

Most of the polymers have non degenerate state and interchanging of single/ double bond changes the system energy. One example of such polymers is polythiophene with ground state of aromatic configuration where double bonds are located in aromatic ring. By changing the double and single bond positions quinoid configuration with higher energy forms. In polymers with non-degenerate state, soliton is not charge carrier. Upon removal or addition of electron to polymer chain, cation/anion radical forms and causes local deformation (within 3-4 monomer) in polymer chain. Figure 1-7 is schematic illustration of neutral aromatic state, positive polaron and positive bipolaron and their associated band diagram. Formation of polaron, creates two energy level in the band gap. Further removal/addition of electron from polaron creates other polarons and when concentration of polarons are high in conjugated polymer, bipolaron forms by coupling of two polaron 15-18.

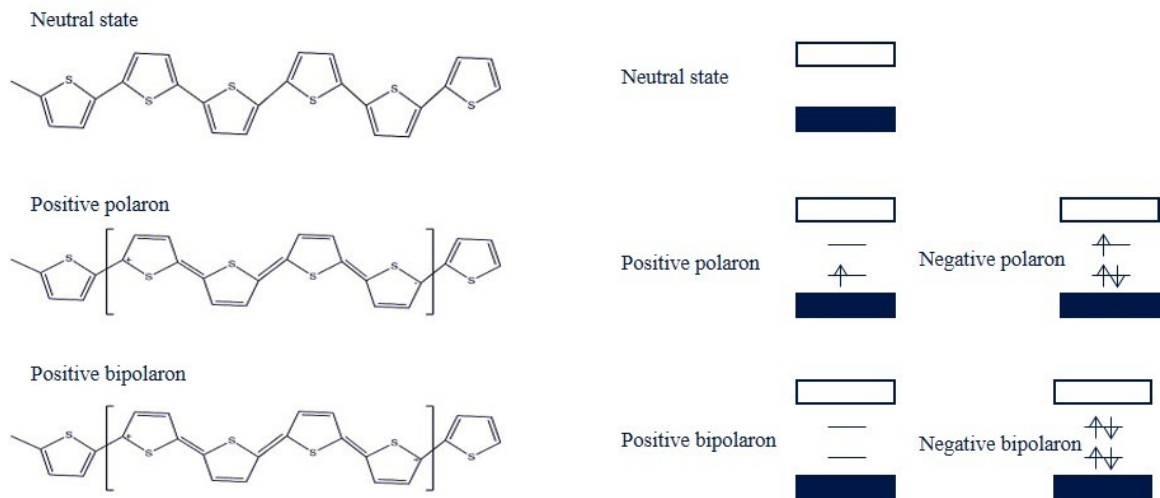


Figure 1-7 Schematic of neutral aromatic state, positive polaron and positive bipolaron and their associated band diagram

Along polymer bulk and film, charge should transport within each polymer chain and also between chains. Solitons and polarons/bipolarons can move within one polymer chain, however this motion is restricted between different chains by trapping in defects and localized states. Beside band like charge transfer along highly ordered polymer back bone, charge hopping and tunneling between localized mid-band gap states are two main charge transport mechanism in conjugated polymers. Unlike band-like conductivity, charge transfer by hopping is temperature dependent and the conductivity increases with temperature. Charges transport within the polymer chain and hops between π -orbitals of adjacent chain. Tunneling become active charge transfer mechanism in low temperature in doped polymers with conducting regions within amorphous background. In this case, charge transfer within densely packed metal like grains are band like and between these regions is via hopping/ tunneling¹⁵⁻¹⁸.

1-2-4 Poly (3 4-ethylenedioxythiophene)-Poly (styrene sulfonate)

Poly (3 4-ethylenedioxythiophene) (PEDOT), is one of the most studied polymers in conducting polymer family. It shows good electrochemical and electrical properties and is stable in wide range of pH. In its neutral state, it is insoluble in most of the common solvents and oxidizes rapidly in air and is unstable. To improve its conductivity and process ability PSS can be added to it. PEDOT: PSS is a degenerately doped p-type semiconductor where holes on PEDOT are compensated by acceptors (SO_3^-). Figure 1-8 shows the chemical structure of PEDOT: PSS.

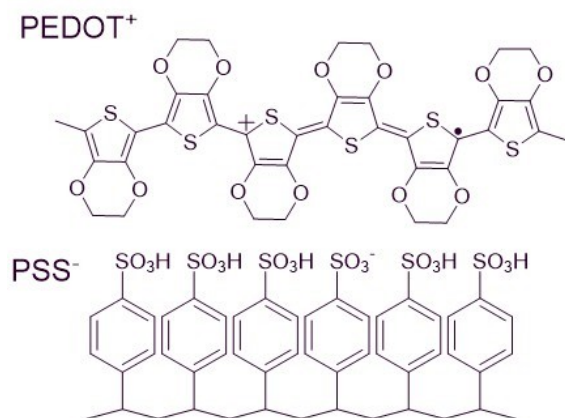


Figure 1-8 chemical structure of PEDOT: PSS hole (positive polaron) on PEDOT balance by SO₃⁻ ion of PSS chain

In electrochemical reaction PEDOT: PSS can undergo oxidation/reduction reaction and switches between conducting (oxidized) state of PEDOT⁺ and semiconducting (neutral) form of PEDOT[°] based on below reaction; where M⁺ represents the ion in the electrolyte:



In PEDOT: PSS, counter ions (anions) can move into and out of polymer film in order to compensate for electronic charge. So the polymer can reversibly change its conductance. In this study PEDOT: PSS has been used as electroactive polymer in organic based transistor^{19,20}.

1-3 Organic transistors

By invention of transistor at 1947, the field of electricity transformed and now transistors are building block of modern electronics. Conventional transistors, utilize inorganic semiconducting materials. However, by development of conducting polymers,

new class of transistors, organic transistors, introduced by Tsumura ²¹. Application of organic transistors expanded recently mainly because they are flexible, soft, cheap, transparent, biocompatible and conduct both electrons and ions which makes them suitable for sensing applications. Organic transistors can be classified into two type of organic field effect transistor (OFET) or organic electrochemical transistor (OECT). Operating mechanism in OFET is based on electrostatic charging while OECT is working based on electrochemical doping/ de-doping.

1-3-1 Organic Field Effect Transistor

OFET is three terminal device consists of source, drain and gate electrodes. Most OFETs are Thin Film Transistors (TFT). Conducting channel between source and drain is organic semiconductor and is separated from gate electrode through gate dielectric. Source electrode is usually grounded and drain and gate voltage is applied relative to the ground. A gate voltage controls the source-drain current. Applying a negative voltage to the gate (V_G) electrode of p-type channel, leads to accumulation of positive charge carriers and formation of p channel at the interface of semiconducting polymer and gate dielectric. Negative voltage between source and drain (V_{SD}), push the holes from source to drain. By increasing V_{SD} , the current between source and drain (I_{SD}) increases till pinch -off point and drain current reaches saturate level (I_{SAT}). OFETs are usually normally OFF transistors and operates in the accumulation mode, where increase in gate voltage causes source-drain voltage to increase²².

One advantage of organic transistors is bio compatibility and the ability to be used as biosensors. Most OFETs can operate by the voltage near 20 V which is very high. In order to reduce the operating voltage one way is to utilize high- κ dielectric materials. However, this will reduce the bio compatibility and ease of fabrication. To overcome this issue, electrolyte has been employed as the gate insulator and gating media. There are several reports on using ionic liquids^{23,24}, ion gels^{25,26}, polymer electrolyte^{27,28} and polyelectrolytes^{29,30} as gate insulator. By applying negative bias to gate, ions will be redistributed in electrolyte and cations move towards the gate electrode, while anions move towards the organic semiconductor. This leads to accumulation of the positive charge carriers at the electrolyte/ semiconductor interface. This migration and rearrangement, causes electrical double layer (EDL) formation on both surfaces (gate/electrolyte and channel/electrolyte). The EDL acts as a capacitor and its capacitance is inversely related to charge separation. As ions are soluble in electrolyte, the EDL's thickness is very small and there is a huge capacitance across it. So the device can operate at very low potential^{23,31,32}. Figure 1-9 shows a formation of double layer and ion/potential distribution along gate and channel.

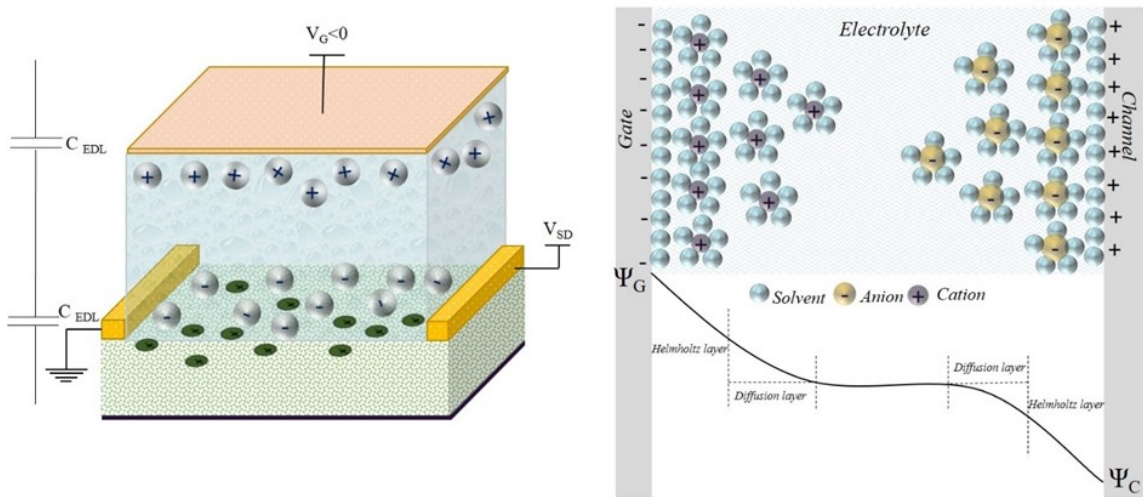


Fig 1-9 a) formation of EDL at gate/electrolyte and channel/electrolyte surface b) ion (above) and potential (below) distribution in Helmholtz and diffusion layer

If the ions of electrolyte penetrate into organic semiconductor and cause electrochemical doping/ de-doping of channel, then the transistor is no longer OFET.

1-3-2 Organic Electro Chemical Transistor

When electrochemical doping/de-doping of the channel, modulate the current between source and drain, then organic transistor is called organic electrochemical transistor. OECT was first demonstrated in the study of poly (pyrrole) based transistor by White et al.³³ Similar to OFETs, OECTs are also three terminal devices in which source-drain current is controlled by application of gate potential across electrolyte. Application of gate voltage modulates the ion motion between electrolyte and channel and in turn alters its conductance by doping or de-doping. In devices which organic materials act as active material, both

electrons and ions can be considered as charge carriers. By oxidation and reduction process in OECTs, the conjugated polymer gets doped or de-doped and the electronic structure and conductivity of the polymer changes. Hence electrochemical transistors work based on transportation of ions and electrons/holes through the active material. In general, OECTs can operate in accumulation or depletion mode. If the polymer channel is doped, an OECT is normally in the ON state. By applying gate voltage ions from electrolyte can enter the film and bringing the transistor to OFF state by de-doping the channel. Since small amount of ions can turn transistor off, these devices operate at low voltage. Figure 3 shows a schematic of a depletion mode OECT working principle.

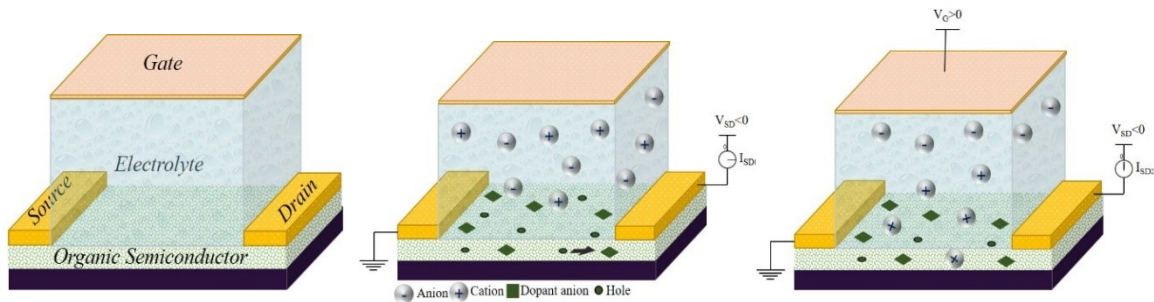


Fig 1-10 Schematic of OECT behavior a) OECT components. b) OECT without gate voltage applied. c) OECT with gate voltage (V_G)

As is shown in Figure 10-1-b, voltage is applied to the drain (V_{SD}) relative to ground and the current through channel (I_{SD}) is measured as a function of applied gate voltage (V_G). It is observed from Fig 10-1-c that by applying positive voltage to the gate, electrolyte's cations are injected into the channel which in turn decreases the source-drain current by de-doping of the channel material.

One of the most employed conjugated polymers in OECTs, is PEDOT: PSS. The OECT based on PEDOT: PSS operates in depletion mode and unbiased channel is effectively “ON”. By applying positive bias via gate electrode, cations of electrolyte are injected in to the polymer and de-dope it. This turns the device “OFF” by decreasing channel conductivity. In these devices, small amount of gate bias causes a significant change in drain current, which is characteristic of electrolyte-gated transistors^{20,34–36}.

Bernards et al.³⁵ modeled the behavior of OECTs. They explain that these devices consist of two circuits; electronic and ionic. The electronic circuit is related to the hole transportation between source and drain and is based on Ohm’s law. The ionic circuit is determined by ion transportation between channel and electrolyte. The interaction of these two is the fundamental of OECT behavior.

1-3-3 OECT based Sensors

There is significant research being conducted in the field of biosensing to develop high sensitivity sensors for detection of low concentration of biomolecules and pathogens and measure low amplitude brain signal. Also, considerable effort is being put on developing selective sensors to distinguish between analytes. Among different biosensing techniques, electronic sensing benefits from being label free and therefore is fast and economical. One example of these sensors is electrochemical sensors based on oxidation/reduction of each analyte. Although effective, this technique suffers from low signal to noise ratio. Therefore, active and biocompatible devices can be used to detect biomolecules both in vitro /ex vivo

and in vivo. A promising technique to overcome other techniques limitation is OECT based biosensors.

In OECT based sensors organic channel (conjugated polymer) acts as a transducer. However, it is not essential that the channel is the part that responds to the analyte. Kumar et al.³⁷ classified the OECTs based on their detection mechanism as :

- i) Direct chemical sensing and chemical state change of channel
- ii) Change in source-drain current by electrolyte- analyte interaction
- iii) Physical deformation of active channel upon binding to analyte and
- iv) Cascade of events in presence of analyte which cause chemical state change of channel.

Therefore, in sensory application of OECTs beside electroactive channel material, gate electrode and electrolyte are also important^{31,37}.

In order to have sensitive sensor based on OECT transconductance of channel should be high. Devices with high transconductance produce large response by small change in analyte. Transconductance of this device relates the amount of change in drain current based on change in gate voltage

$$g_m = \Delta I_D / \Delta V_G \quad (1-2)$$

Where g_m is the transconductance, ΔI_D is the change in drain current and ΔV_G is the change in gate voltage^{20,38,39}. The simplest biosensor based on OECT, could be ion sensor. As described earlier, variation in ion concentration alters the OECTs behavior (source-drain current) and therefore can be used as ion sensor^{40,41} and ion selective sensor^{42,43}.

One other type of biosensors based on OECT is enzymatic sensor which react to analyte upon change in the pH of electrolyte or change in gate voltage. In these type of sensors, enzyme catalyze the oxidation reaction of analyte and therefore respond to change in H^+ concentration. Alternatively, hydrogen peroxide as product of enzymatic reaction will oxidize on gate electrode and change the gate voltage by transferring electron to gate. Using this technique glucose⁴⁴ , uric acid⁴⁵ and lactate⁴⁶ have been measured. Nucleotide and charge biomolecules can also be detected using OECT. In vicinity of the channel because of charged nature of biomolecules, they attract ions with different charge and therefore limit the amount of ions entering to the channel. Thus, the effective gate voltage needed for the transistor to operate will increase. E. Coli⁴⁷ and DNA⁴⁸ sensors are example of these type of sensors. As OECT has a rapid response to change in ion flow, it is promising to conduct in electrophysiology where each heart beat will change the effective gate voltage⁴⁹ and neuron recording⁵⁰.

1-4 Objective of this work

Fundamental understanding of characteristics of OECT makes it possible to design devices which covers one needs. OECTs are promising tools to study brains chemical and electrical states in minimally invasive method than conventional neural probes with needles. It can be fabricated using simple fabrication tools on flexible substrates with high density of measuring sites compared to conventional one terminal electrode based devices. Active three terminal sensors make it possible to record many neurons at a time due to their compact and dense structure. Furthermore, organic channel of these sensors makes

functionalization and introducing functional groups to the channel relatively easy. This makes future neuro-probes a step forward by making them selective through functionalization of the channel with neuro-receptor.

To achieve this high end of neuro-probes first step is to understand the working principle of OECT in order to design sensors with high sensitivity and high speed. So in this work the aim is to fabricate OECTs on flexible substrate and study its mechanism to help for better design of future neuro-probes. Moreover, study on the effect of channel material structure and its impact on OECTs working principle, helps to define specific channel material for specific application all within one simple treatment. Furthermore, over oxidized PEDOT: PSS as channel of OECT will be investigated to understand its function as ion sensor. The possibility of having over oxidized PEDOT: PSS as an ion pump next to PEDOT: PSS based OECT will put the sensing and treatment devices in one platform. All together this work one step to understand brain better and helps to better design of neuro-probes.

1-5 Outline of thesis

In this chapter a brief introduction on history and chemical/electronic structure of conjugated polymers, nature of charge carriers and charge transmission in conducting polymers is presented. Moreover, electrolyte gated transistors and organic electrochemical transistor and its application in biosensing is introduced. Chapter 2 covers the experimental procedure for OECT fabrication and PEDOT: PSS characterization techniques as well as OECT's electrical characterization. Chapter 3 outlines the major of OECT device

characteristics. In this chapter effect of device geometry and channel thickness on its operation parameters e.g. transconductance, ON/OFF current ratio, threshold voltage, capacitance per unit volume extracted from total amount of charge introduced into the channel are presented. In Chapter 4 effect of over oxidation on PEDOT: PSS structure is presented. Spectroscopy techniques are used to explain structural changes in PEDOT: PSS and OECTs with over oxidized PEDOT: PSS will be introduced. Summary and future work are presented in Chapter 5.

2 Experimental procedure

In this chapter, the fabrication procedure of OECT device used in the research is presented. Electrical characterization techniques are also presented here. Along with this, the PEDOT: PSS film characterization are also described.

2-1 OECT device fabrication

Whole fabrication step of OECT is shown in figure 2-1. Each step will be discussed with more detail in this chapter.

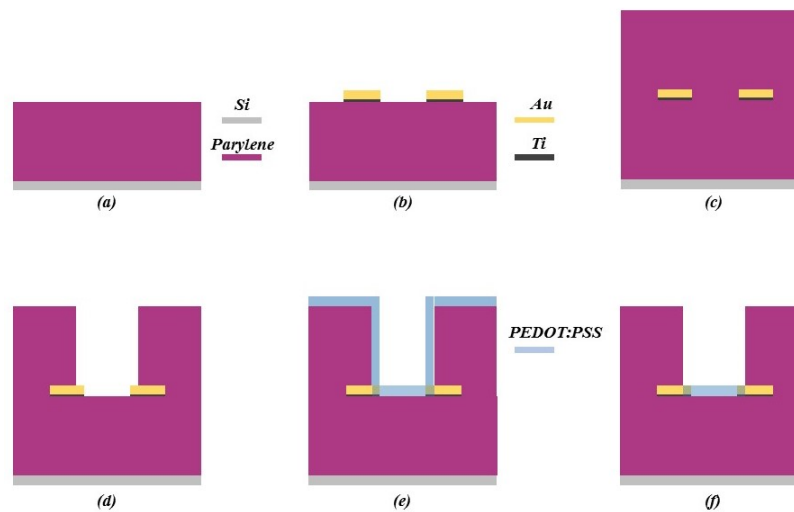


Figure 2-1 (a) Parylene deposition (b)Source, drain and contact pad deposition (c)Parylene deposition to insulate electrodes (d) channel and gate opening (RIE) (e) channel and gate coating (f)PEDOT: PSS patterning (The schematic is not to scale)

Fabrication starts with Parylene deposition which has been utilized as substrate of devices. Parylene is a family of Poly-para-xylylene which is used in coating applications.

Parylene film is flexible, light and pinhole free, insulator, biocompatible and chemically stable. Parylene deposition was done by SCS/PDS 2010 Parylene coater. Figure 2-2 summarize the deposition process of Parylene-C.

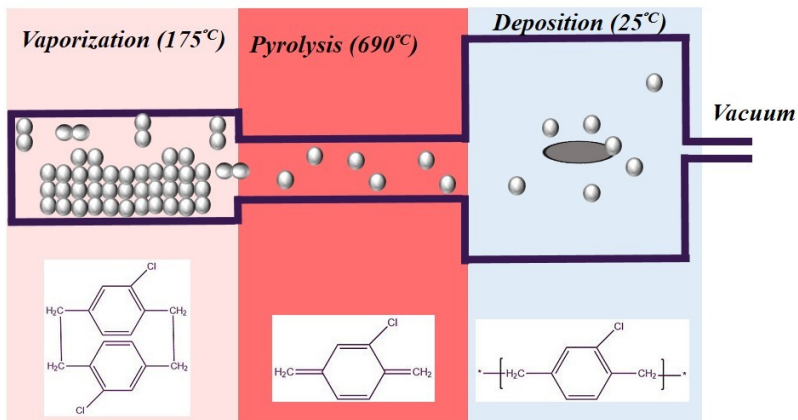


Figure 2-2 Deposition process of parylene-C

The deposition process happens at low vacuum (~ 0.5 Torr) and starts with dimer vaporization at 175°C . Later on, the dimer gas goes through pyrolysis reaction at 690°C and gaseous monomer forms. Monomer enters the deposition chamber which is hold at room temperature and condensed on the surface. the excess and unbound monomer trapped at liquid cold trap. The thickness of Parylene film was measured using Alpha step profilometer and was kept constant at $3\ \mu\text{m}$ throughout the experiment.

Gold has been used as source, drain and measurement pads as well as for interconnects. Au has been used in organic transistors as contact extensively because it forms an ohmic contact with organic semiconductor⁵¹. All photomasks were designed using L-Edit software. Figure 2-3 shows the layout of designed mask and device /pad layout.

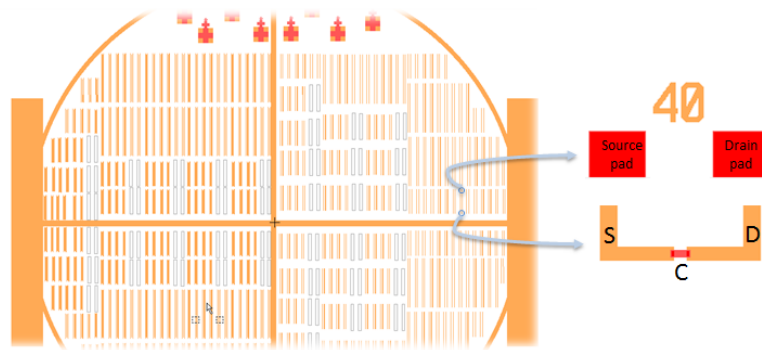


Figure 2-3 Designed photomask layout for different steps of optical lithography

Optical lithography (ABM mask aligner) and AZ 5214 negative photoresist have been utilized to pattern photoresist for contact deposition. Ti/Au with thickness of 10/100 nm has been deposited using magnetron sputtering technique. Finally, contacts were patterned by lift off in acetone. Another layer of 3 μm parylene has been deposited to insulate all interconnect gold contacts from electrolyte.

Second step of optical lithography (Quintel 4000 mask aligner) has been done to pattern channel area and source/drain pad. HPR 506 with final thickness of 2.5 μm has been used as photoresist. Parylene was etched from channel and measurement pads using Reactive Ion Etching (RIE) (plasma lab micro etch) technique. Oxygen with flow of 100% and pressure of 150mT and power of 100 W has been used. It was found that high pressure and power cause Parylene removal from silicon substrate at some regions. By above mentioned parameters 18 minute was enough to etch out the parylene. If parylene would not etch fully there won't be any contact between source/drain and semiconducting polymer. To make sure parylene was fully removed electrical contact was measured on gold openings and ohmic I-V curve was obtained.

Later, thin film of PEDOT: PSS has been spin coated (Laurell WS-650) as electroactive channel material. Aqueous solution of PEDOT: PSS is commercially available with different conductivities (1-1000 S/cm). Clevios PH 100 Heraceus PEDOT: PSS has been used as base solution for channel mixture. It has been found that polar organic solvents improve PEDOT: PSS conductivity by forming hydrogen bond with PSS and introducing change in its structure^{52,53}. Therefore, ethylene glycol (Sigma) was added by 20 v/v % to the mixture. 0.1v/v % of dodecylbenzene sulfonic acid (Sigma) also added to the mixture to adjust surface tension and to minimize contact resistant⁵⁴. (3-glycidyloxypropyl) trimethoxysilane (Sigma) was also added by 0.9 v/ v% amount to the mixture as cross linker. Measurement results of Stavrinidou et al.⁵⁵ demonstrate that PEDOT: PSS is an efficient ion transformer in biological environment but ion mobility decreases as hydration decreases. So there is a limit between stability of film in aqueous media and ion transportation. By using cross linkers although stability of film will increase but the ability to up take water and ion mobility decreases. It is worth mentioning that the I did not study the effect of change in amount of above mentioned mixture and used it constant throughout the research. The mixture then was mixed under nitrogen flow in an aluminum foil covered vacuum flask to prevent PEDOT: PSS cleavage, as it is air and light sensitive. Samples were spun at different spin rate to obtain film with different thickness. After spin coating samples were cured at 130°C for 15 minutes on hot plate covered with petri dish. Using an oven to cure the samples at the same temperature and time resulted in samples which were over crosslinked and their conductivity decreased. This was measured by testing PEDOT: PSS film using four-point probe. Devices were left in DI-water for 15 minutes to remove

any unbound PEDOT: PSS and dried thoroughly using nitrogen gun. A related point to consider is to make sure all HPR 506 is removed from previous step as PEDOT: PSS reacts with it.

PEDOT: PSS has acidic nature and it is not possible to pattern it with conventional acid sensitive photoresist. Acid sensitive photoresists are affected by acidic PEDOT: PSS and PEDOT: PSS films are damaged by standard developers. Taylor et al.⁵⁶ developed hydrofluoroethers based photoresist for PEDOT: PSS patterning. So in this study, to pattern PEDOT: PSS and to protect channel and pad area, fluorinated ORTHOGONAL OSCoR 4001 negative photoresist^{57,58} and OSCoR 103 developer have been used. The resist is yet at experimental phase so the parameters for patterning were obtained. Also, it was found that is not very stable. To remove the unwanted area, first, I tried oxygen plasma but the etch rate of resist in oxygen was too high (900nm/min) which makes it difficult to withstand whole etching process. So I used bleach as an oxidizing agent to oxidize and deactivate the unwanted PEDOT: PSS area. Before stripping the resist, the resistance of the deactivated area was measured using four-point probe ($\sim 1.0E+9$).

In most OECT reports, PEDOT: PSS has been patterned using sacrificial layer of Parylene where a layer of soap (micro 90) used as anti-adhesive layer for peeling the sacrificial layer of Parylene and after channel area definition, Parylene etched by RIE and the sacrificial layer removed after PEDOT: PSS spinning. However, based on what I tried, PEDOT was also peeling with sacrificial layer and contacts were poor because of remaining soap. The fabrication step and devices fabricated by this technique is presented

in Appendix A. Figure 2-4 shows confocal microscope image of OEECTs. All the fabrication steps recipes are presented in appendix A.

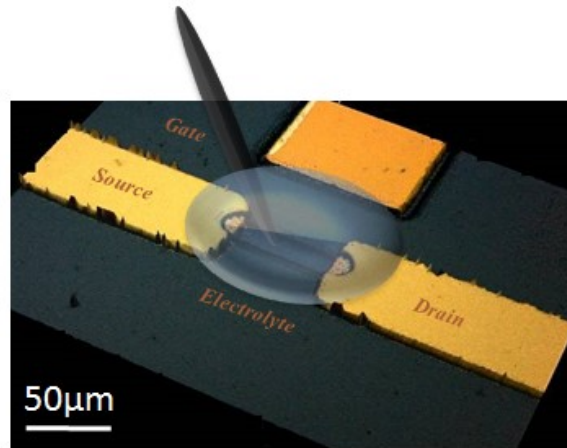


Figure 2-4 confocal microscope image of OEECT

2-2 Electrical measurement

A Keithley 4200 SCS parameter analyzer was utilized to carry out the electrical measurements. The current between source and drain was measured with sweeping the voltage between source and drain at different gate voltage and $I_{DS}-V_{DS}$ curve obtained for the transistors. Furthermore, the current between source and drain obtained by sweeping gate voltage at different source/drain voltage and device transconductance has been measured. Finally, by pulsing gate voltage, gate transient current at different V_G has been measured and the area under the curve has been used to determine the total amount of charge injected to the channel. All characterizations were conducted using 100mM NaCl in DI water as electrolyte and an Ag/AgCl wire (Warner instrument) as gate electrode. For

all I-V measurements the source measure unit (SMU) of Keithley and for all pulse measurements pulse measurement unit (PMU) have been used.

To study the effect of over oxidation PEDOT: PSS film or OECT devices immersed in conventional Clorox bleach for 15 second and rinsed thoroughly with DI water and dried under nitrogen.

2-3 PEDOT: PSS film characterization

2-3-1 Ellipsometry

Spectroscopic Ellipsometry has been used to determine film thickness and optical properties of the film. In spectroscopic ellipsometry the reflected wave's phase and amplitude is measured and compared with the incident wave. And raw spectroscopic ellipsometry data is converted into two parameters the phase change, Ψ and the amplitude ratio, Δ . Then the acquired data model using a mathematical model to obtain lowest mean square error and film parameters will be extracted based on the assigned model. In this study, Ellipsometer (J.A. Woollam M-2000V) has been used to obtain change in phase and amplitude of the incident light and Complete EASE v4.50 software (J.A. Woollam Co. Inc.) is used to analyze the ellipsometry data.

2-3-2 Four-point probe

Four -point probe (Lucas labs) has been used to measure PEDOT: PSS film resistance. Five measurements have been done at different points of sample and the average has been

used. Four- point probe applies current to the two outer probe and the voltage difference is measured between two inner probe. Thin film sheet resistance can be calculated as $4.532 \times V/I$. This is valid only for the films with thickness less than probe spacing.

2-3-3 XPS/UPS

X-ray photoelectron spectroscopy (XPS) has been used to define chemical composition of pristine and over oxidized PEDOT: PSS film. XPS is an analytical surface analysis technique to study chemical composition and chemical/ electronic states of elements. It measures the kinetic energy and intensity of the emitted photoelectrons to analyze chemical composition of the sample. XPS measurements were done using XPS Kratos AXIS 165 and monochromatic Al $K\alpha$ source ($h\nu = 1486.6$ eV). The spectrometer was calibrated using the binding energy (84.0 eV) of Au 4f_{7/2} with reference to the Fermi level and the surface charging effects was counterbalanced with using a charge neutralizer. CasaXPS software has been used for data analysis. Peaks have been identified based on NIST standard reference database for XPS and all peaks have been shifted with respect to standard C-C peak at 284.8 eV.

To study electronic structure of pristine and over oxidized PEDOT: PSS film, UV-photoelectron spectroscopy (UPS) has been used. UPS were measured using He I line irradiation ($h\nu=21.2$ eV). The power of UPS was 30W and samples were biased at -10V during measurements to observe the secondary electron edge. CasaXPS software has been used for data analysis.

2-3-4 Raman spectroscopy

The effect of conformation change of PEDOT chain by over-oxidation was studied by Raman spectroscopy. Raman spectroscopy utilizes an monochromatic light to study the molecular vibration of the sample. A monochromatic light shines on the sample and inelastically scattered light with shifted frequency is used to determine vibration energy of the sample. Raman analysis can be used to study the doping behavior of conjugate polymers. Raman spectra were recorded by Nicolet Almega-XR Raman microscope excited by a 785 nm laser source.

3- Organic Electrochemical Transistor, characteristics and operation mechanism

3-1 Introduction

The field of conducting polymers and mainly organic electrochemical transistors have been investigating for bioelectronics applications. Advantages such as conformability, high quality electrical contact, ease of fabrication and biocompatibility made OECTs a great potential of future bio diagnostic tools. The operating mechanism of OECT is different and yet there are few studies on its operation fundamental. Based on solid state theories, Prigodin.et.al.⁵⁹, explained the transistor behavior in OFF state to be related to limited hole concentration, far charge hopping distance and low hole mobility by introducing cations to the polymeric channel. However, the study did not focus on experimental device working principle. Tu.et.al.⁶⁰, also studied the electrolyte gated field effect transistor behavior but they just reported transient behavior of device based on four capacitance coefficient and charge model. In another model, Coppede.et.al.⁶¹, focused on different ions transfer from electrolyte to the channel and modeled the effect of diffusion on OECT behavior. Yet the best presented model for OECT behavior is Bernards-Malliaras model³⁵. The model describes OECT operation in terms of electronic and ionic circuits, where electronic circuit is based on Ohm's law for hole transportation between source and drain. The ionic circuit accounts for ion transport in the electrolyte which itself depends on polarization at the channel/ electrolyte and gate/electrolyte interface. Based on Ohm's law for p type

semiconductor, the current flux will be based on equation 3-1 and models the electronic circuits.

$$J(x) = q \cdot \mu \cdot p(x) \cdot \frac{dV(x)}{dx} \quad (3-1)$$

Where J is current flux, μ is hole mobility, q is elementary charge, dV/dx is electric field and $p(x)$ is hole density. By applying positive gate voltage, cations are injected to the semiconducting channel and compensate one acceptor. therefore, effective dopant density (p), is related to initial hole density (p_0) and the amount of charge which is injected to the channel (Q) to the known volume (v) of it based on equation 3-2.

$$p = p_0 \cdot \left(1 - \frac{Q}{q \cdot p_0 \cdot v}\right) \quad (3-2)$$

To solve device current behavior, total injected charge from slice of channel with area of ($w \times dx$) in position x is related to the capacitance per unit area (c_d) (equation 3-3) in which $V(x)$ is spatial voltage profile.

$$Q(x) = c_d \cdot w \cdot dx \cdot (V_G - V(x)) \quad (3-3)$$

By combining equations 3-1 to 3-3 we obtain the effective dopant density as equation 3-4 where V_p is pinch off voltage and d is channel thickness and current flux as equation 3-5.

$$p(x) = p_0 - \frac{c_d \cdot w \cdot dx \cdot (V_G - V(x))}{q \cdot w \cdot dx \cdot d}$$

$$V_p = \frac{q \cdot p_0 \cdot d}{c_d}$$

$$p(x) = p_0 \left(1 - \frac{V_G - V(x)}{V_p} \right) \quad (3-4)$$

$$J(x) = q \cdot \mu \cdot p_0 \left(1 - \frac{V_G - V(x)}{V_p} \right) \frac{dV(x)}{dx} \quad (3-5)$$

Integrating equation 3-5 from source to drain then gives

$$I = G \left[1 - \frac{V_G - \frac{1}{2}V_D}{V_p} \right] V_d, \quad G = q\mu p_0 w \cdot d/l \quad (3-6)$$

This model is based on uniform hole mobility throughout the channel and disregards the effect of carrier concentration on hole mobility. Friedlein et.al.⁶² recently modified the model for non-uniform hole mobility.

In this Chapter, first PEDOT: PSS film's characterization will be discussed and then OECT results based on PEDOT: PSS will be presented. Channel thickness effect on main OECT parameters will be explained and the device capacitance will be extracted from total amount of charges injected to the channel and hole mobility calculated based on OECT's model.

3-2 Results and discussion

3-2-1 PEDOT: PSS film characterization

To study PEDOT: PSS film optical properties and thickness of the films, spectroscopic Ellipsometry has been used. Figure 3-1 shows the Ellipsometry model of the film and obtained refractive index (n) and extinction coefficient (k) at incident light of $\theta=65^\circ$.

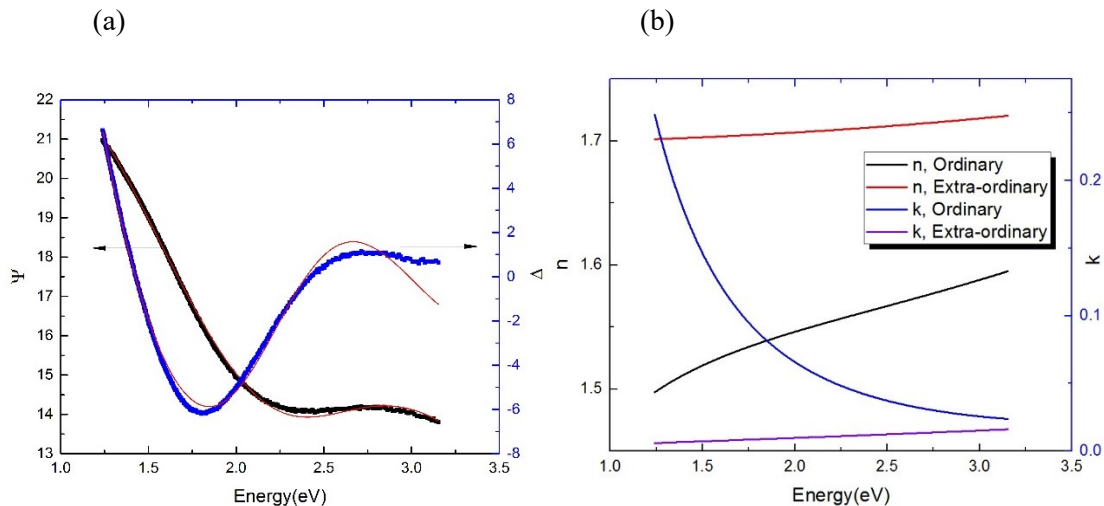


Figure 3-1 (a) experimental Ψ and Δ data and the assigned optical model (red line) and (b) uniaxial anisotropic of refractive and extinction coefficients

Previous studies of PEDOT: PSS shows the anisotropic optical^{63,64} and conductivity^{65,66} behavior. Therefore, uniaxial anisotropic model has been used to study the film behavior. The optical model consists of Drude and Lorentz oscillator found to best fit to the data as the model considers the anisotropy. The in-plane and out of plane resistance and film roughness was fixed and final fitted model showed mean square error (MSE) of 2.37. The obtained n and k is similar to the previous reports⁶³, where, out of plane optical parameters are not changing significantly at different light wave length.

Film thickness for different spin rates have been measured using Ellipsometry spectroscopy and modeled by the same above model. Figure 3-2 shows the film thickness with respect to the different spin coating rate. It is obvious that by increasing spin rate final films with lower thickness will be obtained. It should be noted that other mechanical

techniques, like step height measurement, have been used and showed thickness values in same order. However, because of soft nature of polymer, optical measurement was found to be more accurate and did not damage the films.

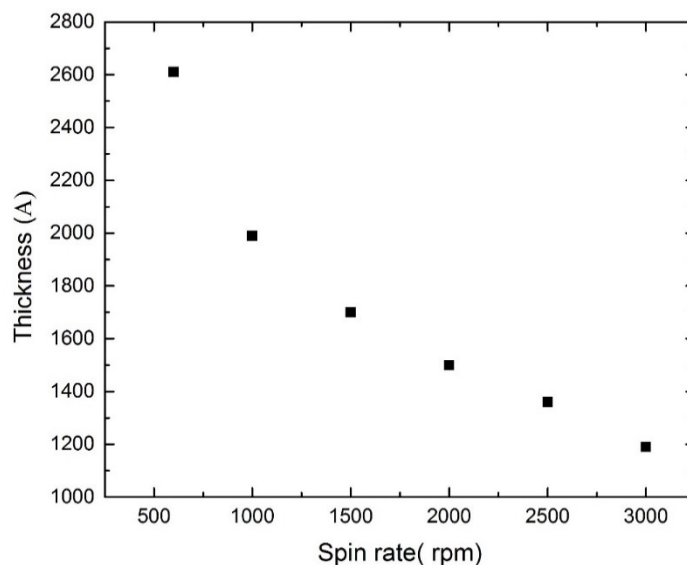


Figure 3-2 PEDOT:PSS film thickness at different spin coating rates

Figure 3-3 shows the PEDOT:PSS film resistance and its associated conductivity for different thickness measured by four point probe. Films with higher thickness result into more conductive films. For the film with thickness of 260nm, conductivity of 550 S/cm has been obtained which is relevently high value ^{64,67-69} using PH-1000 clevios PEDOT:PSS. However, one can improve conductivity further by post solvent treatment using methanol or ethylene glycole^{68,70}. Post solvent treatment removes excess PSS regions, which act as shells for PEDOT flakes, and increase conductivity.

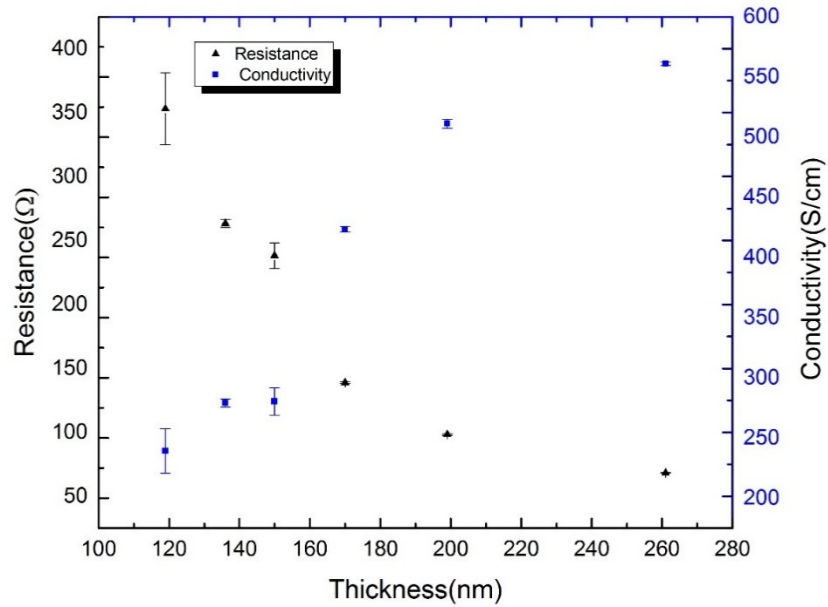


Figure 3-3 change in resistance and conductivity of PEDOT: PSS film by its thickness

3-2-2 OECT device operation

OECT devices have been fabricated in different length (5-50 μm) in two different widths (10 and 20 μm) to study the effect of device geometry on its performance. Figure 3-4 shows schematic device layout and output IV characteristics of OECT with $w=20\mu\text{m}$, $l=40\mu\text{m}$ and $d=260\text{nm}$.

Channel conductance measured at zero gate bias found to be 35 S/cm which is drastically low compared by film conductance. This significant difference in conductance of the device as compared to the film can be attributed to the device fabrication steps and particularly final PEDOT: PSS patterning step using orthogonal resist and bleach. But it could also be due to the not good overlap of the channel with the gold contacts. In spite of

change in conductance of channel compared to film conductivity, the device shows high enough ON current compared to other organic transistors. for PEDOT:PSS based OECT the ON current range reported is as low as $1\mu\text{A}$ ⁷¹ ($w=100\ \mu\text{m}$ and $d=180\text{nm}$) to as high as $2\ \text{mA}$ ⁷² ($w=50\ \mu\text{m}$, $l=50\ \mu\text{m}$, $d=500\text{nm}$) and therefore that is not an issue in our experiments.

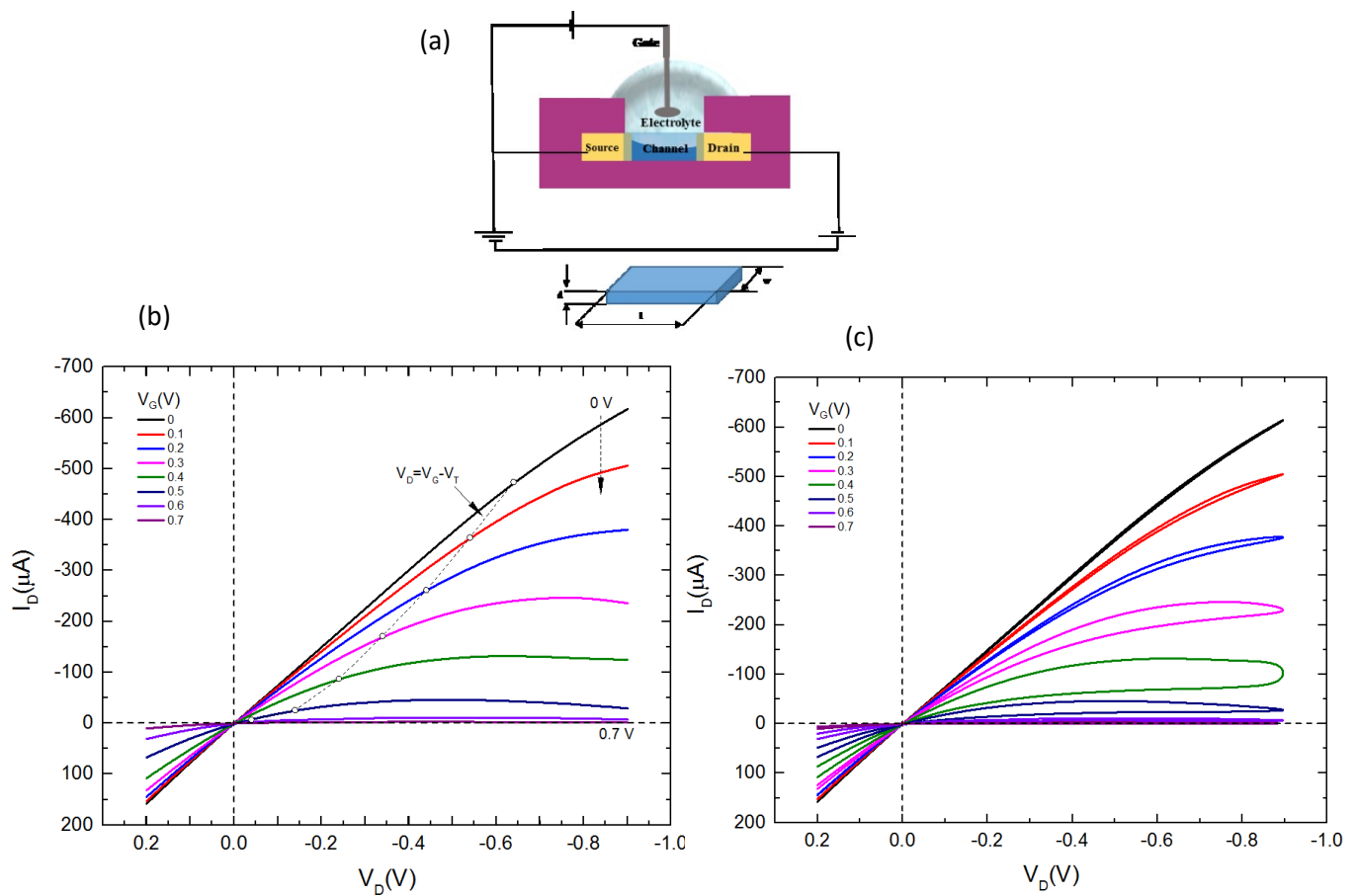


Figure 3-4 (a) schematic layout of device and channel geometry and (b) output characteristics of the device with dimensions of $w=20\mu\text{m}$, $l=40\mu\text{m}$ and $d=260\text{nm}$. V_G changing between 0 (top curve) to 0.7 V (bottom curve) (c) output characteristics of device with hysteresis indication

By applying negative bias between source and drain, hole as charge carrier, conducts charge and by increasing voltage between source and drain, current increases till it reaches a maximum and then saturates. This demonstrates a typical I_D - V_D family of curves for a depletion transistor, normally ON. By applying positive voltage to the gate electrode, cations from electrolyte enter the channel and compensates hole and therefore reduce the current between source and drain. It is observed from figure 3-4-b, 0.7V gate voltage is enough to turn the OECT completely OFF ($I_D=-1.7\mu\text{A}$ at $V_G=0.7\text{V}$, $V_D=-0.9\text{V}$) and this is hallmark of electrolyte gated transistors. Because of high electrolytic capacitance the voltage required to operate the device is low. Figure 3-4-c is indication of hysteresis for the device. As it is clear, the hysteresis increases by increasing the gate voltage to the voltages near threshold voltage and decrease again. In the voltages near threshold voltage large number of cations push to the channel by gate bias and therefore the hysteresis increases. This trend was observed for all other measurements in this study. Gate current was in order of nA in all the experiments which shows very low gate leakage. The dashed line separates the linear and saturation region of OECT.

Figure 3-5 shows the OECT transfer curve and transconductance for two V_D of -0.6V and -0.1V for the same device.

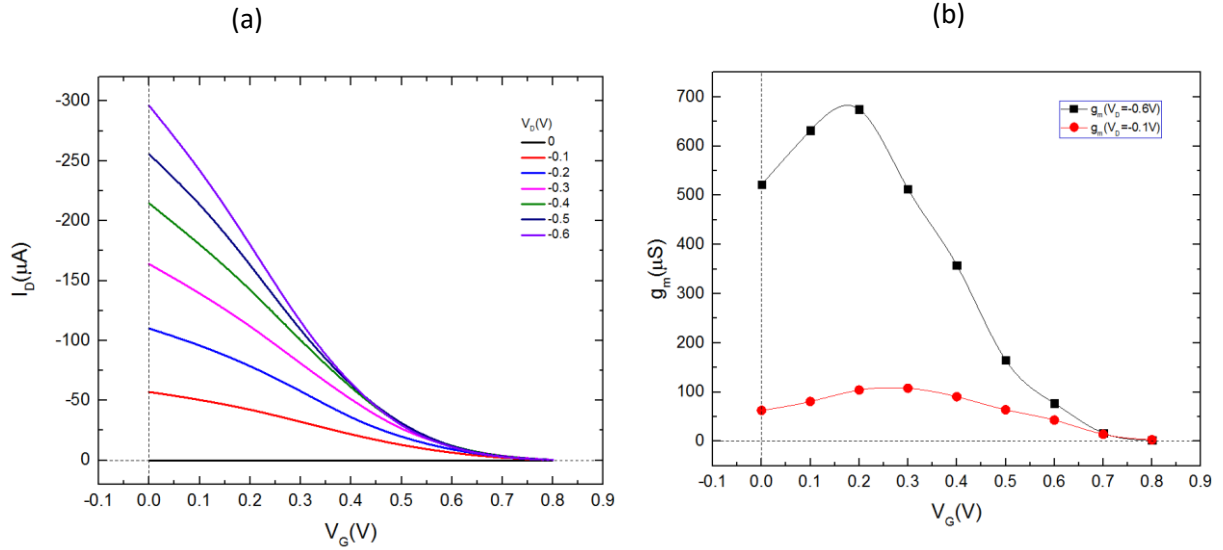


Figure 3-5 a) transfer curve for V_D changing from 0 (bottom curve) to -0.6V (top curve) and OEECT transconductance for V_D of -0.6v (top curve) and -0.1V (bottom curve) for the device with dimension of $w=20\mu\text{m}$, $l=40\mu\text{m}$ and $d=260\text{nm}$.

Transfer curve of OEECT shows by increasing drain voltage from 0V to -0.6V, the current between source and drain shifts to larger values. However, by increasing V_D more, the amount of change in current decreases. Also the transfer curves show by increasing gate voltage, OEECT turns OFF by decreasing charge carrier concentration ($I_D=-0.2\mu\text{A}$ at $V_D=-0.6\text{V}$ and $V_G=0.8\text{V}$) and therefore increasing gate bias more will not change I_D .

Transconductance relates magnitude of gate voltage to change in source-drain current and its curve in Figure 3-5 shows typical transistor behavior. By increasing gate voltage transconductance reaches a maximum at effective gate voltage and above certain limit, transistor turns OFF. At higher drain voltage, transconductance increases and reaches its maximum at threshold voltage (V_T) and by increasing drain voltage even more the transconductance will not change. Here, the above mentioned device, reaches its maximum

transconductance ($700 \mu\text{S}$) at $V_G=0.2\text{V}$ and $V_D=-0.6\text{V}$. OECT's transconductance value depends on gate electrode and channel geometry. By changing device geometry one can tune transconductance and reach to maximum transconductance value at low gate voltage. Figure 3-6 shows transfer curve and transconductance for the device with same width ($20\mu\text{m}$) and same thickness (260nm) and different length ($20\mu\text{m}$). As it is obvious from the curve, maximum transconductance ($1073 \mu\text{S}$) is obtained at zero gate voltage. Consequently, it is possible to engineer device to achieve desirable characteristics.

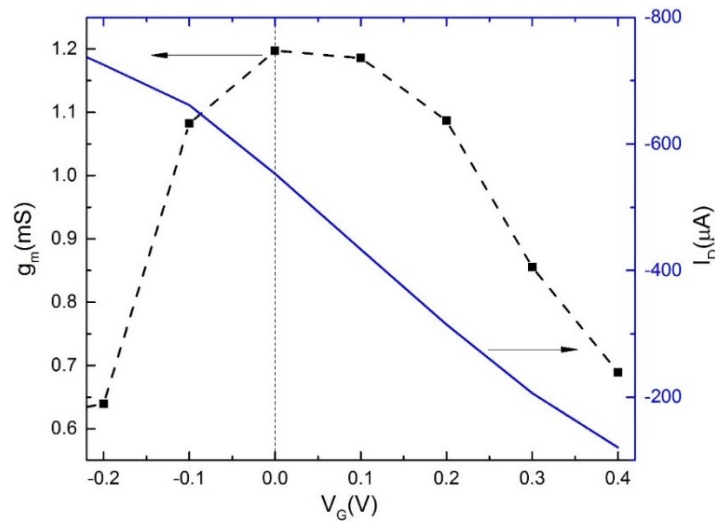


Figure 3-6 transfer and transconductance curve of the OECT for the device with dimension of $w=20\mu\text{m}$, $l=20\mu\text{m}$ and $d=260\text{nm}$ at $V_D=-0.6\text{V}$

Figure 3-7 demonstrates the device geometry relation to its transconductance. For the devices with same thickness ($d=260\text{nm}$) and width ($w=20\mu\text{m}$) the transconductance increase with decreasing the length from $l=50 \mu\text{m}$ to $l=10 \mu\text{m}$. Furthermore, the gate voltage which cause maximum transconductance shifts to lower voltage. Figure 3-7-b shows almost linear w/l relation with transconductance. This was anticipated from device

behavior equations as well (equation 3-6). Hence for biosensing applications, having a larger w/l of channel would be an advantage to obtain higher sensitivity. High transconductance of OEET makes them good candidate for biosensing applications where, small change in gate voltage cause large change in current. There are other studies⁷³⁻⁷⁵ to increase transconductance of flexible electrolyte gated transistors but OEETs based on PEDOT: PSS has the largest value of transconductance²⁰ (4020 μS) reported so far. The transconductance value normalized to the volume of channel is 10^{14} S/m^3 for the highest transconductance reported compared to 4×10^{13} S/m^3 for this study.

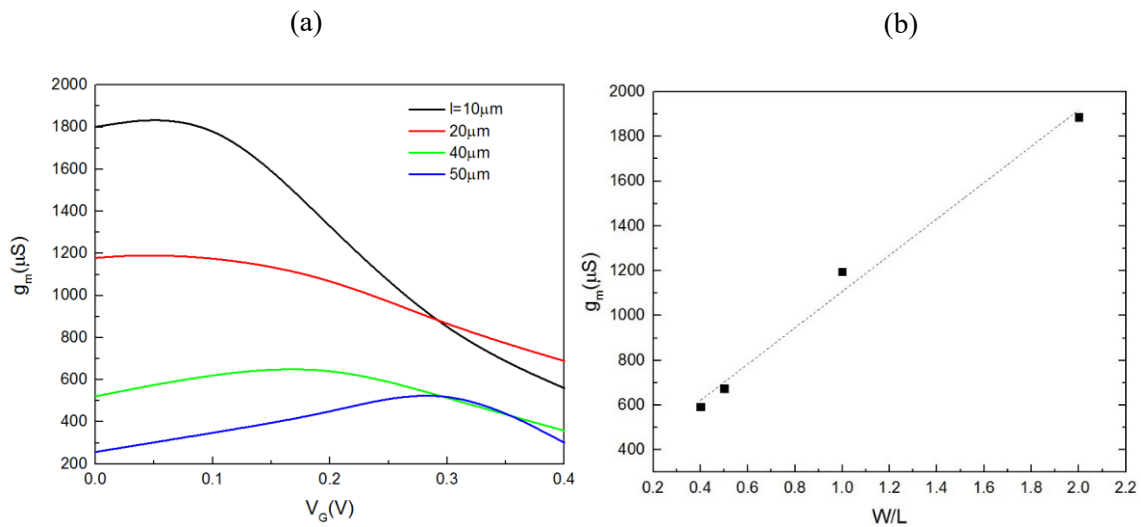


Figure 3-7 transconductance as a function of device geometry all measurements have been done at $V_D = -0.6\text{V}$ ($d=260\text{nm}$)

In depletion mode transistor, threshold voltage (V_T) is the voltage which needs to be applied to the gate to turn the transistor OFF. When drain voltage is higher than $V_{\text{DSAT}} = V_G - V_T$, the I_D saturates and OEET operates in saturation region. At saturation, drain current

is related to square of V_{DSAT} . Threshold voltage is 0.64V which it was used to define saturation region at figure 3-4. ON/OFF current ratio of OECT and threshold voltage of device has been calculated using transfer behavior of device ($w=20\mu\text{m}$, $l=40\mu\text{m}$, $d=260\text{nm}$ at $V_D=-0.6\text{V}$) and is shown in figure 3-8. It is anticipated that by increasing the area of the device, higher gate voltage is needed to turn the OECT OFF and therefore V_T will increase. For the device with same width ($20\mu\text{m}$) and $l=50\mu\text{m}$ the threshold voltage is 0.77V and for the device with $l=20$ the threshold voltage is 0.54V compared to 0.64V of device with $l=40\mu\text{m}$. The $I_{ON/OFF}$ ratio for the device is 2×10^3 (Average of ON/OFF ratio of five different devices are 1.1×10^3) Typically, this ratio for organic transistors is low compared to inorganic ones mainly due to their low ON current. For the device with similar geometry Hutter et.al reported 1×10^2 ⁷¹, Kumar et.al reported 5.5 ⁷⁶ and Rivnay et.al reported 10^5 ³⁴ for the $I_{ON/OFF}$ ratio . However, the ratio can be improved by modifying fabrication technique.

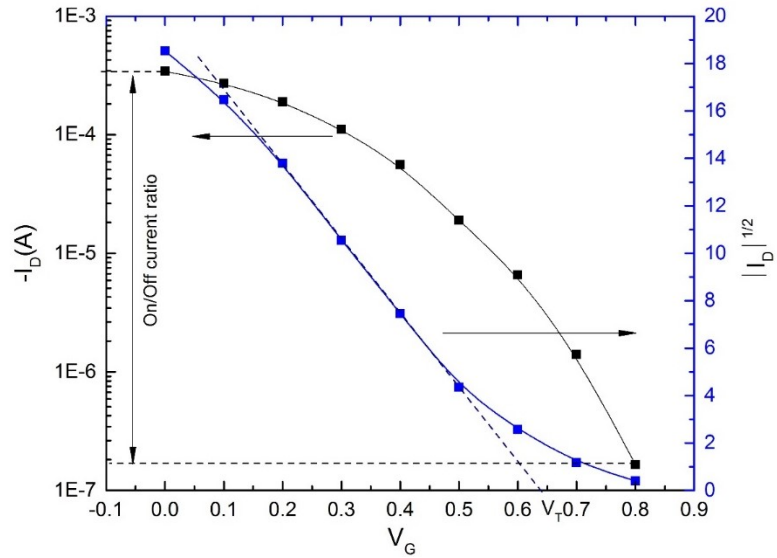


Figure 3-8 transfer characteristics with indication of ON/OFF current ratio and threshold voltage for the device with dimension of $w=20\mu\text{m}$, $l=40\mu\text{m}$ and $d=260\text{nm}$ at $V_D=-0.6\text{V}$

Furthermore, mechanical deformation effect on OECT device was tested. The device was peeled off from silicon substrate and crumpled as in Figure 3-9 and un-crumpled device has been measured again. Device characteristics shows that such harsh handling cause 20% less device ON current. However, this can be improved by increasing base parylene thickness to some extent.

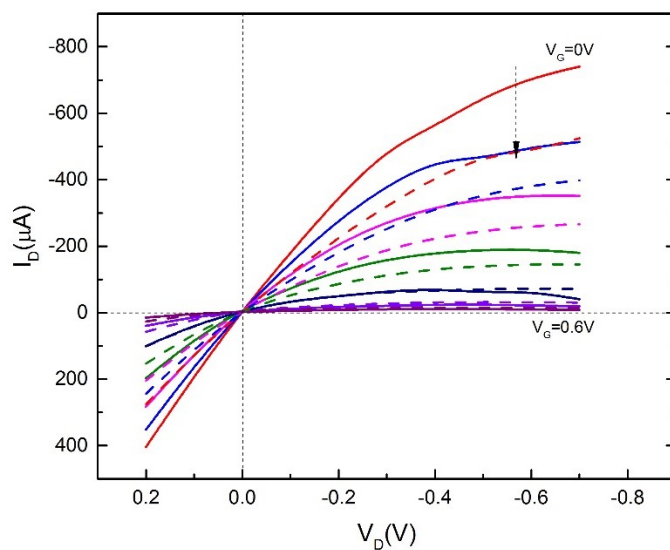
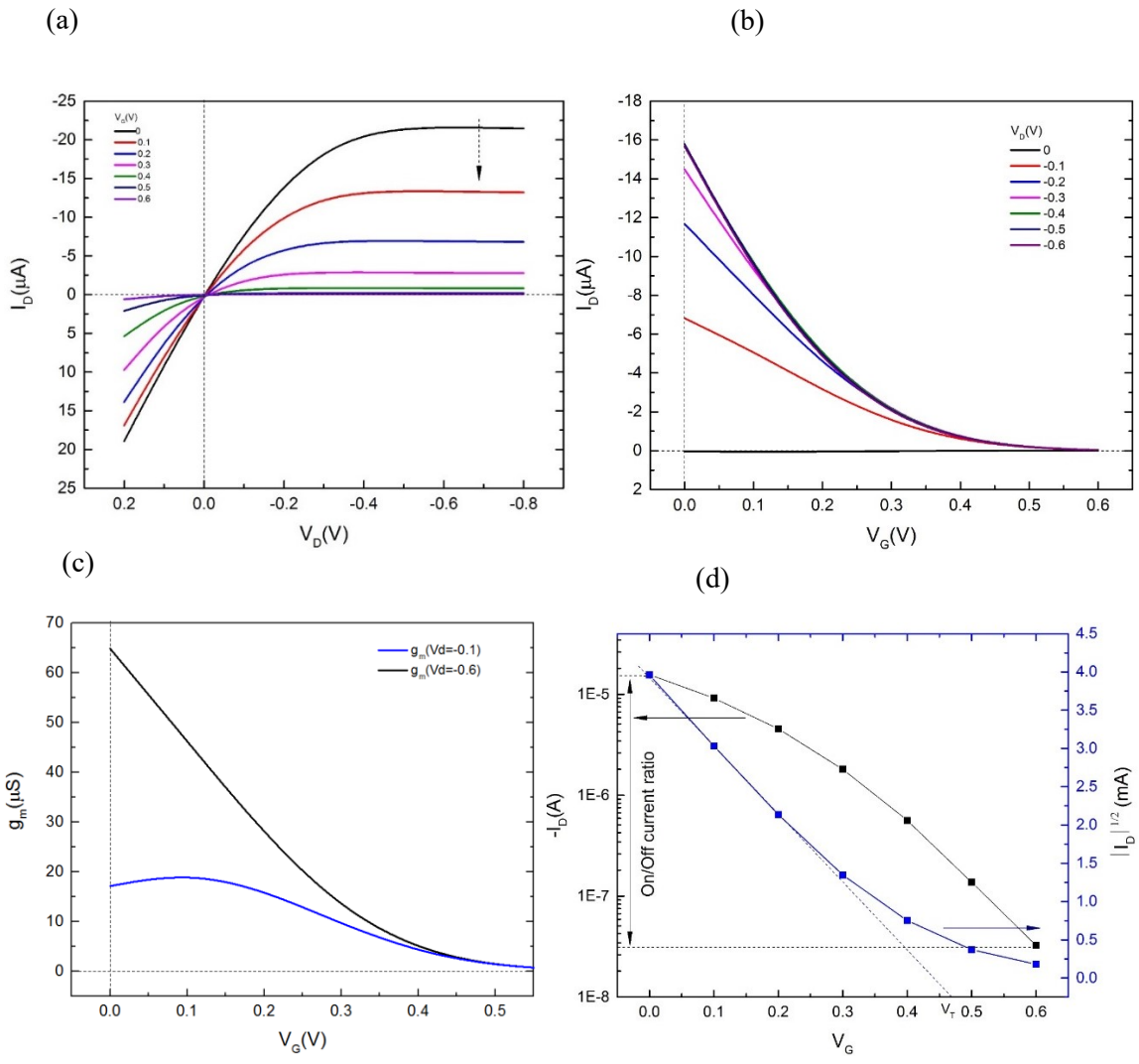


Figure 3-9 crumpled device and its output characteristics before being peeled and after being peeled and crumpled ($w=10\mu\text{m}$, $l=30\mu\text{m}$, $d=260\text{nm}$)

To this point, effect of device width and length on its response has been explained. OECT works on ions penetration to the channel and de-doping it by compensations of hole. Therefore, channel thickness also has major role in device performance. It is expected to see high ON current and high transconductance in thick channel compared to thinner ones. However, it may take longer time for thicker channel to de-dope and this reduces the response time. As a comparison OECT with channel thickness of 170nm has been studied and compared with OECT data with channel of 260nm. Figure 3-10 summarize the thin device characteristics.



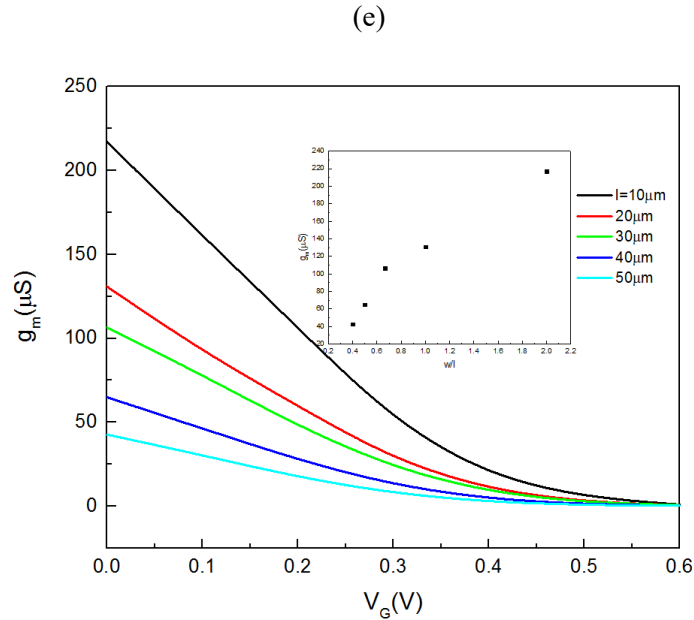


Figure 3-10 a) output characteristics of the device. V_G changing between 0 (top curve) to 0.6 V (bottom curve) b) transfer curve for V_D changing from 0 (bottom curve) to -0.6V (top curve) c) and OECT transconductance for V_D of -0.6v (top curve) and -0.1V (bottom curve) d) transfer characteristics with indication of ON/OFF current ratio and threshold voltage e) transconductance as a function of device geometry for V_D of -0.6v for the device with dimension of $w=20\mu\text{m}$, $l=40\mu\text{m}$ and $d=170\text{nm}$ at $V_D=-0.6\text{V}$

Figure 3-10 (a) shows the output characteristics of OECT with thinner channel device. When compared with Figure 3-4 (270nm thick channel), it is clear that the device ON current at zero gate voltage is lower for the thinner channel device. The result was anticipated based on four-point measurement study. It has been found⁷⁷ that in the thinner films of PEDOT: PSS, the separation between PEDOT phase occurs and therefore the hopping distance increases and limits film conductivity. Beside low current range between source and drain, the linear operation region is limited and it saturates in lower source-drain voltage. This is due to the small volume of channel which needs to deplete by ion penetration as well as lower number of charge carriers between source and drain. Figure 3-10 (b) shows the transfer curve of the OECT at different V_D changing from 0V to -0.6V. The current trend is similar to the thicker channel device (Figure 3-5) and it reduces by

increasing the gate voltage. Though, the increasing drain voltage more than -0.4V , does not affect the current between source and drain. This again emphasizes the lower threshold voltage which is needed to turn the device OFF compared to the thicker channel OECT. Comparing Figure 3-5 and 3-10 (c) shows significance difference in transconductance. Film thickness plays significant role in determining device transconductance. In thin films, because of lower film density and lower crystallinity⁷⁸⁻⁸⁰, the distance between PEDOT regions is far and therefore the charge transfer and therefor transconductance is limited. Also in OECTs with thinner channel high transconductance reaches at lower gate voltage. Recently Rivnay et.al. studied the effect of device thickness on its behavior and their results published in Science Journal⁷². Hole mobility and capacitance per unit area are two parameters which affect transconductance. PEDOT: PSS film structure and crystallinity has main effect on hole mobility and therefore thick films with high degree of crystallinity has better hole mobility. However, in contrast to hole mobility, high capacitance needs the structure which can easily uptake water from electrolyte and conducts ions with ease. Therefore, mixture of these two parameters define transconductance and thickness effect on it. Subsequently, one can design sensors with combination of high transconductance (thick channel OECT) and fast response time (thin channel OECT).

Figure 3-10 (d) shows the ON/OFF current ratio and threshold voltage. Because the volume of channel is lower in this thin channel OECT, the gate voltage which is needed to deplete channel is lower (0.55V compared to 0.64V). Furthermore, because the ON current is less therefore, the ON/OFF current ratio is low (480) (average of ON/OFF of five different device is 475) . Table 3-1 summarize the main device parameters for two devices

with different thicknesses (260 and 170nm) and same channel length (40 μ m) and width (20 μ m). Figure 3-10 (e) shows effect of device geometry on its transconductance. The trend is similar for the devices with thickness of 260nm and 170nm and by increasing the w/l ratio the transconductance increase from 42 μ S (w/l=20/50) to 217 (w/l=20/10).

Table 3-1 OECT characteristics for two different channel thickness and same length and width (w=20 μ m and l=40 μ m)

<i>Channel thickness (nm)</i>	<i>Transconductance (μS) ($V_D=-0.1V$)</i>	<i>Transconductance (μS) at saturation ($V_D=-0.6V$)</i>	<i>Threshold voltage(V)</i>	<i>ON/OFF current ratio</i>
260	108 ($V_g=0.3V$)	700 ($V_g=0.2V$)	0.64	2.1×10^3
170	19.92 ($V_g=0.1V$)	64.89 ($V_g=0V$)	0.55	4.8×10^2

3-2-3 OECT operation model

In conventional transistors, gate dielectric and its capacitance per unit area has major role in device operation. There are several studies on gate dielectric material which can be thick enough to minimize the current leakage and has high relative permeability to compensate the thickness effect on capacitance. One main advantage of electrolyte gated transistor is its high capacitance which allows the device to operates in low voltage. Recent investigation shows capacitance of PEDOT: PSS based OECT to change with channel volume^{72,81}. Based on Helmholtz model for double layer capacitance, capacitance per unit area of electrode is in order of 10 μ F/cm². By applying positive bias to gate, capacitor forms between injected cation and sulfonate groups of PEDOT on channel.

To measure specific capacitance, injected charge has been measured at different gate voltages. To do so, constant voltage of -0.5V has been applied between source and drain and gate electrode has been pulsed between 0V and different voltages (0.01-0.7V). Figure 3-11 (a) shows the schematic of device measurement setup. Figure 3-11(b) shows gate current transient from the OEET at different applied gate voltages. By increasing gate voltage, the amount of charge injected in the channel increases and the area under the curve. Total charge injected from electrolyte through biasing gate electrode to the channel has been measured from area under the curve. The inset in figure 3-11(b) shows the typical pulse voltage form.

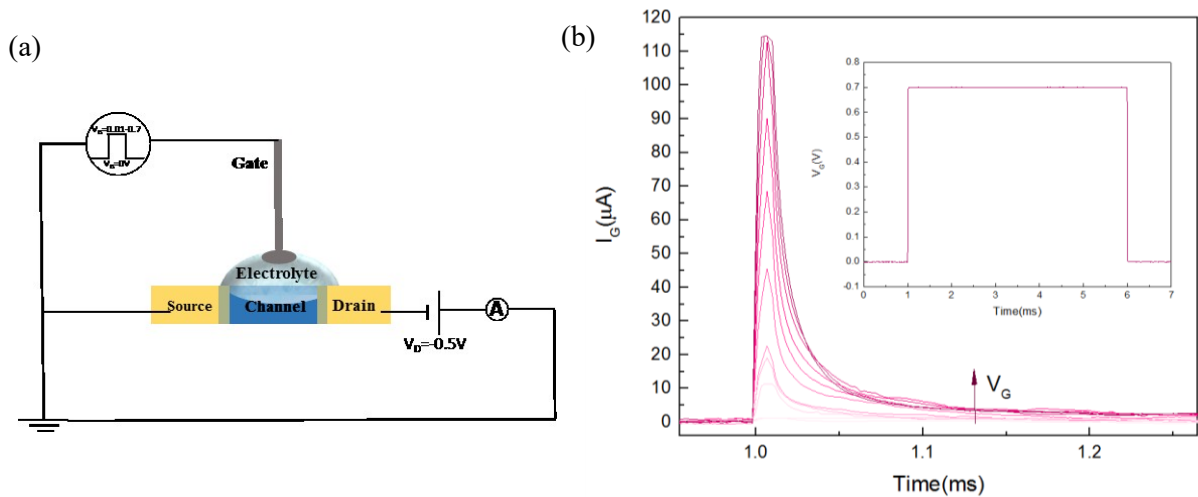


Figure 3-11(a) schematic of device measurement, (b) Gate current transient from an OEET with dimensions of $w=10\mu m$, $l=40\mu m$ and $d=260nm$ and the inset is an image of pulse voltage applied to the gate

Figure 3-12 shows linear trend for the charge and gate voltage (with $r^2=0.988$) and the slope of the line is a measure of capacitance yielding a capacitance of $5.94\pm 0.2 nF$ ($dQ=C.dV_g$).

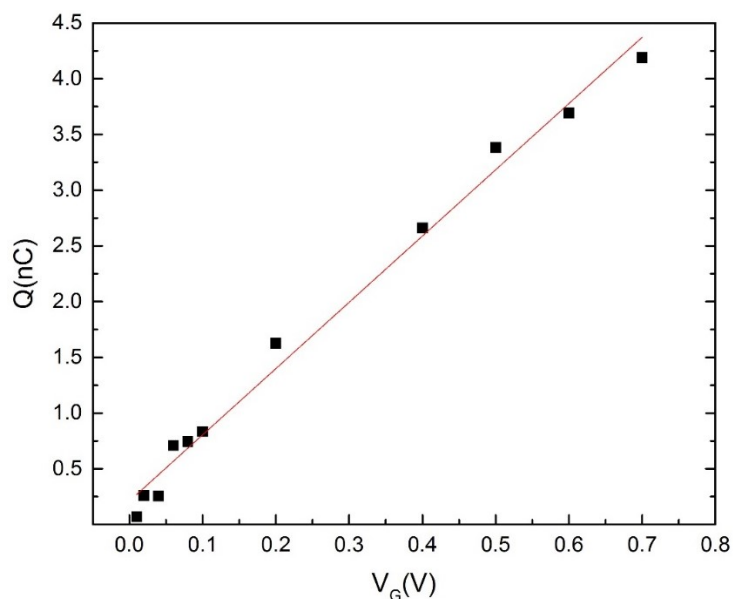


Figure 3-12 injected charge as a function of gate voltage for OEET of $w=10\mu\text{m}$, $l=40\mu\text{m}$ and $d=260\text{nm}$

Capacitance per unit volume of the OEET then is $57.11 \pm 1.92 \text{ F/cm}^3$. This is a very high number for PEDOT: PSS based OEET. Rivnay et.al.⁷² calculated the capacitance the same way that I did and obtained capacitance with value of 41.7 F/cm^3 ($w=50\mu\text{m}$, $l=50\mu\text{m}$, $d=500\text{nm}$). They also measured electrochemical impedance of the channel and obtained the capacitance value of 39.3 F/cm^3 . In order to increase capacitance hole density can be increased by polymers with high hole density or by introducing nano particles to the polymer structure to minimize the distance between charge sites.

Recently Proctor et.al.⁸¹ modeled the concept of specific capacitance. Based on this model film capacitance is consist of N parallel plate(capacitor) with area of $A=w \times d$ and distance of α . Where α is average distance between charge carriers and $l=N \times \alpha$. Based on Helmholtz double layer model, the capacitance per unit area of the film is

$$C_{dl}' = C_{dl}/A = \epsilon \epsilon_0/t \quad (3-7)$$

Where $\epsilon \epsilon_0$ is relative permittivity and t is distance of charges accumulated on the surface and the plate. Total capacitance of film consist of N parallel capacitance is

$$C = N \epsilon \epsilon_0/t \quad (3-8)$$

Therefore, capacitance per unit volume is inversely related to the distance of charge carriers.

$$C^* = \frac{N \epsilon \epsilon_0}{t(N\alpha dw)} \rightarrow C^* = C_{dl}/\alpha \quad (3-9)$$

In order to calculate the distance between carriers we need to calculate the density of carriers in PEDOT: PSS film. The molecular weight of PEDOT: PSS with the ratio of 1:2.5 PEDOT: PSS is 595g/mol and density of PEDOT: PSS is 1g/cm³. The density of thiophene ring (PEDOT) is 1.01×10²¹(unit/cm³). If holes form for each 3 thiophene ring, then the density of holes is 3.4×10²⁰(unit/cm³) and the distance between charge carriers (α) is 1.44 nm. Double layer capacitance for the polymers is between 1-10 μF/cm² and therefore the specific capacitance should be between 7-70 F/cm³.

Figure 3-13 (a-b) shows OECT output and transfer characteristics. By considering specific capacitance and substituting $V_D = V_G - V_T$ in the equation 3-6, current at saturation will be based on equation 3-10.

$$I_D^{SAT} = \frac{w \cdot d}{2l} \cdot \mu \cdot C^* \cdot (V_T - V_G)^2 \quad (3-10)$$

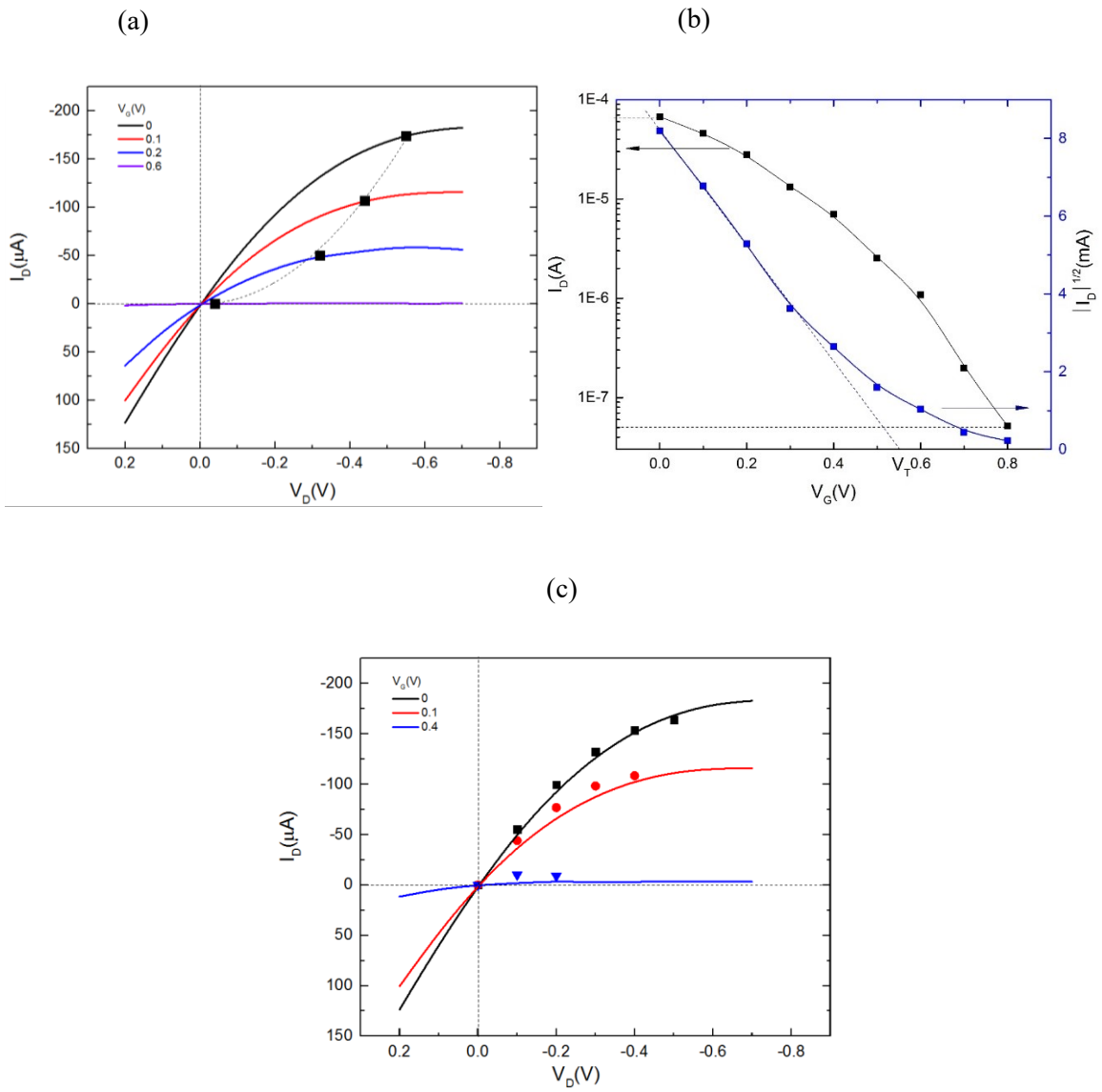


Figure 3-13 output characteristics of the device. V_g changing between 0 (top curve) to 0.6 V (bottom curve) symbols shows the saturation region b) transfer characteristics with indication of ON/OFF current ratio and threshold voltage for the device c) points indication of I_D based on OECT model and real data with dimension of $w=10\mu\text{m}$, $l=40\mu\text{m}$ and $d=260\text{nm}$

Threshold voltage obtained from figure 3-13 (b) is 0.56V. symbols at I_D - V_D curve of figure 3-13 (a) related to $V_D=V_G-V_T$ and associated drain current at saturation. The dashed

line is parabola fit to the data with $r^2=0.99$ and $y=-565\pm 12 x^2$. Hole mobility could be extracted from equation 3-10 to be $3.02 \text{ cm}^2/\text{Vs}$.

$$175.34 \times 10^{-6} = \frac{10}{2 \times 40} \times 260 \times 10^{-7} \times \mu \times 57 \times 0.56^2 \rightarrow \mu = 3.02 \text{ cm}^2/\text{Vs}$$

This high mobility value is because of structure of PEDOT: PSS which it is not too dense and is crystalline enough for charges to move within film. One can measure hole mobility using other techniques such as time of flight of holes across the channel. Using the equation 3-6, current at linear region of diagram has been obtained and shown in figure 3-13 (c). The model is not valid at the regions where $|V_T - V_G| < V_D$. Also after saturation point I_D will fit better to the I_D^{SAT} value. It should be noted that by measuring hole mobility through other experiments one can obtain better model.

3-3 Conclusion

Organic electrochemical transistor with PEDOT: PSS as channel material has been studied. Results show that at devices with higher w/l ratio has higher transconductance. Also study of OECT shows that one can change OECT geometry to obtain high transconductance at low gate voltage and even 0 V. Later the effect of channel thickness on OECT characteristics has been studied and results shows that, thinner channel devices have lower ON current and therefore low ON/OFF ratio (200 compared to 2000 for thick device) because of low crystallinity of PEDOT: PSS structure. Also, threshold voltage in thinner channel OECT is lower because small amount of ions is required to deplete the

channel and turn the transistor OFF. Furthermore, transconductance decreases with decrease of thickness. However, it reaches its maximum at lower applied voltages. In our study device with thickness of 260 nm had its maximum transconductance (700 μS at 0.2V) though device with same geometry and lower thickness (170nm) has its maximum (68 μS at 0V).

Afterwards, specific capacitance has been measured by pulsing gate electrode and measuring its transient current and total charge injected to cation through gate electrode. Specific capacitance found to be 57 F/cm^3 a value which is higher than reported values. Although one should note that this value comes from single sample and might be higher than actual capacitance because of ion accumulation on electrolyte/channel interface. This high capacitance is due to the PEDOT: PSS structure which allows the ion to penetrate in and out while keeping its high conductivity through PEDOT regions. Using this value for capacitance, mobility value derived from OECT model to be $3.02\text{cm}^2/\text{Vs}$.

4 -Oxidation Effect of PEDOT: PSS Channel Material on Combined Depletion and Accumulation Regime OECT

4-1 Introduction

The electroactive material used for organic devices is conducting or semiconducting π -conjugated polymer. Employing this type of materials in electronic application offers numerous advantages over conventional inorganic technology, mainly in the matter of ease of fabrication, mechanical flexibility, cheap and low temperature processing. The conductivity and functionality of organic molecules can be adjusted by reduction-oxidation chemistry. This property of conjugate polymers allows conversion of ionic current to electronic current and makes them a good candidate for bio-electronic applications. In these type of devices, a biological event alters conductivity of the polymer and transduces it into an electrical change. PEDOT: PSS is a widely used conjugate polymer in organic devices. In PEDOT: PSS structure, PEDOT chain has been p-doped by withdrawing electrons from polymer backbone. Through this oxidative doping process, charge carriers (polaron and bipolaron) forms and positive doping charges carried by PEDOT are balanced by the counter anion (PSS⁻). However, the doping is reversible and in an electrochemical reaction, PEDOT: PSS can undergo oxidation/reduction reaction and switches between conducting (oxidized) state of PEDOT⁺ and semiconducting (neutral) form of PEDOT[°]. This structure conducts both electrons and ions and ions can move into and out of polymer film to compensate for electronic charge^{19,82}. Although doping/de-doping process is reversible, when PEDOT: PSS film is subject to severe oxidizing environment, an over-oxidation

occurs and alters the conductivity of polymer by changing its structure. Figure 4-1 shows the proposed over-oxidation mechanism in presence of sodium hypochlorite (bleach) as a strong oxidizing agent. This mechanism shows multiple oxidization steps by binding oxygen to the sulfur atom in the thiophene ring and sulfur eliminating by formation of sodium sulfate^{83,84}.

So far the reported OECTs based on PEDOT: PSS as channel material, operates in depletion mode, normally ON devices. In these devices the unbiased channel is effectively ON and by applying positive bias via gate electrode, cations of electrolyte are injected in to the polymer, compensate the sulfonate groups of the PSS and depletes the hole on PEDOT chain. This turns the device OFF by decreasing channel conductivity. OECTs can be operate in accumulation mode as well. Although initial studies on OECTs were based on accumulation mode devices^{33,85-87}, yet the field requires more investigation on this type of OECTs. Accumulation mode device consumes less power as it is normally OFF and it is basic of most microelectronic industry. By developing organic based accumulation mode transistor, the present transistor industry can be combined by flexible and low cost electronics. And if these devices used as sensor, in presence of analyte they will turn ON and detect analyte over background signal. Also, developing both depletion and accumulation mode devices using one material will lead to developing logic circuits which will make the technology even more attractive.

In this work, I tune the reduction level of PEDOT: PSS and the possibility of using the oxidized PEDOT: PSS film as channel material for accumulation mode OECT. To the best of my knowledge this is first study on accumulation mode PEDOT: PSS based OECT

which shows by one simple oxidation process, depletion mode OECT can be converted into accumulation mode device. In this study, electrical characteristics of thin PEDOT: PSS film has been reported on both doped and de-doped film and effect of its oxidation state on device behavior has been investigated. This study can open up a way to develop depletion/enhancement mode sensors with high sensitivity and high transconductance as well as high efficiency and signal to noise ratio.

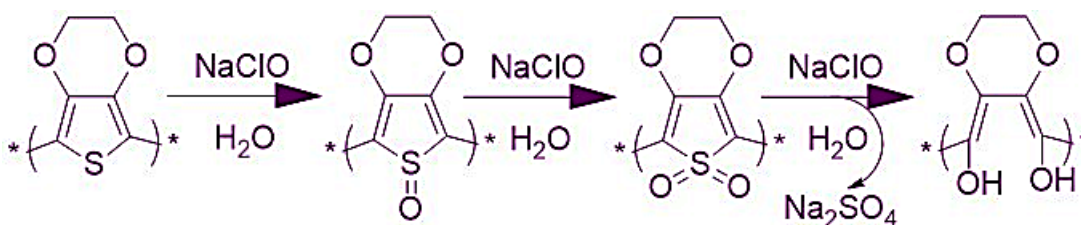


Figure 4-1 Over oxidation process of PEDOT: PSS

4-2 Results and discussion

4-2-1 effect of over oxidation on PEDOT: PSS chemical structure change

Figure 4-2 shows the change in conductivity of PEDOT: PSS film with oxidation time. The effect of over-oxidation on reducing electrical conductivity has been studied before⁸⁴. It can be observed that the conductivity of the polymer drops by six order of magnitude in 10 seconds of over-oxidation.

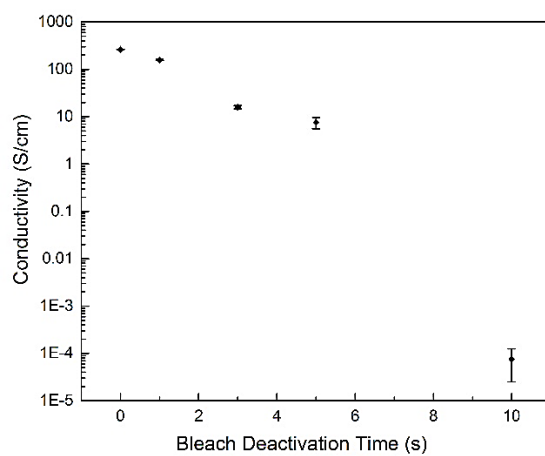


Figure 4-2 change in conductivity of PEDOT: PSS film by different oxidation time

Herein we study the over-oxidation reaction and its effect on PEDOT: PSS structure. Pristine and sodium hypochlorite treated polymer's structure have been compared by XPS and Raman spectroscopy. Figure 4-3 shows high resolution S (2p) and Na (1s) XPS spectra for both pristine and over-oxidized PEDOT: PSS samples.

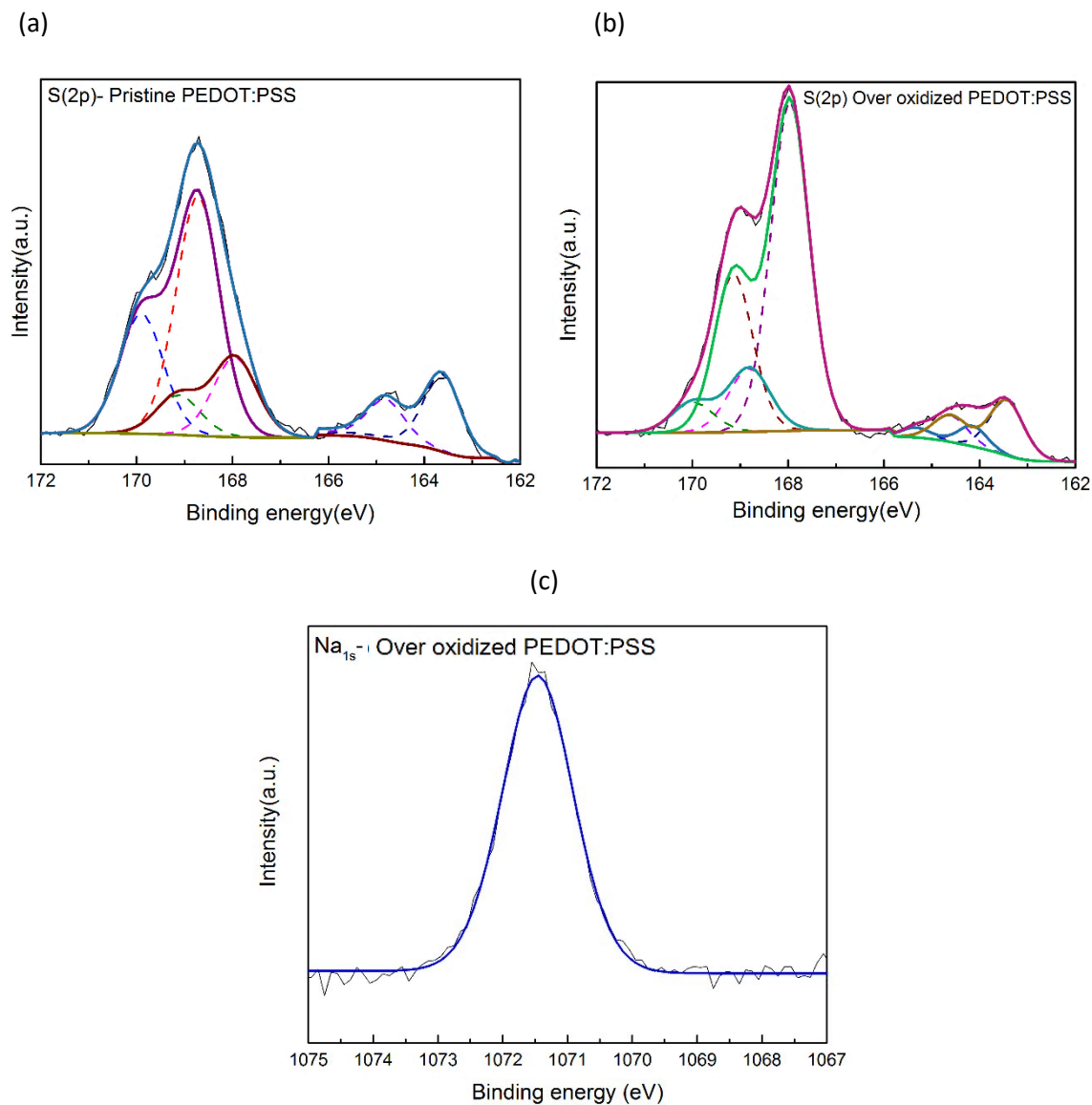


Figure 4- 3 S(2p) spectra of prinstine PEDOT: PSS (a), S(2P) spectra of over oxidized PEDOT: PSS (b) , Na(1s) spectra of over oxidized PEDOT :PSS(c)

Because of spin orbit splitting, sulfur (S) atoms give rise to two contribution of S ($2p_{1/2}$) and S ($2p_{3/2}$) with intensity ratio of 1:2, same FWHM and 1.18 eV energy splitting in S (2p) spectra. Both PEDOT and PSS contain sulfur atom where S (2p) doublet for PEDOT

has lower binding energy compared to PSS. As PEDOT chain is p- doped and positive charge is delocalized over several chain, S (2p) doublet peak of PEDOT is asymmetric with a tail toward high binding energies. In case of PSS derived spectra is composed of two spin split doublet with S (2p 3/2) located at 167.9 eV and 168.6 eV. These peaks can be attributed to $\text{SO}_3^- \text{Na}^+$ and $\text{SO}_3^- \text{H}^+$ respectively. Similar peaks were reported for pristine PEDOT :PSS film before^{52,88}. The relative intensity of S (2p) at PEDOT reduces and the amount of S (2p) doublet at PSS increase in the over-oxidized PEDOT: PSS film. This is observed in the spectra from the over-oxidation film shown at Figure 4-1. During this process, 22.4% of sulfur atoms of PEDOT change chemically and form sodium sulfate on the polymer chain (atomic concentration of S of PEDOT changed from 18.3% to 14.2%). Thus, based on atomic concentration obtained by CasaXPS software for both pristine and over-oxidized sample, the sulfur ratio of PEDOT: PSS changes from 0.22 (18.3 PEDOT/81.7 PSS) to 0.16 (14.2 PEDOT/85.8 PSS). The binding energy of sodium sulfate runs at PSS region of S (2p) spectra (~168 eV) and increases the relative intensity of S peak at higher binding energies. Furthermore, because of possible partial oxidation of PEDOT two doublet of S (2p) is visible in the PEDOT region of spectra.

Sodium (Na) (1s) peak at 1071.5 eV and strong Auger peak at 497.3eV verifies the formation of sodium sulfate by over-oxidation. There were no Chlorine (Cl) peaks detected in survey and high resolution scan of Cl. This eliminates the presence of sodium hypochlorite residue on the sample. XPS study shows shrinking of PEDOT area by over-oxidation reaction and formation of sodium sulfate in polymer chain.

The effect of conformation change of PEDOT chain by over-oxidation was studied by Raman spectroscopy. Raman analysis can be used to study the doping behavior of conjugate polymers. Figure 4-4 compares Raman spectra of pristine PEDOT :PSS and over-oxidized polymer film.

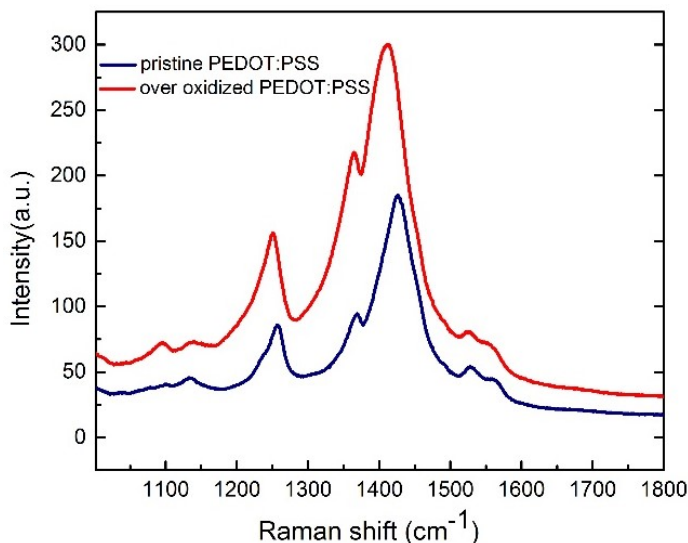


Figure 4-4 Raman spectra of pristine PEDOT:PSS and over-oxidized PEDOT:PSS film

The principle Raman bands for pristine polymer film in Raman spectra are at 1559 and 1529 cm^{-1} which are related to asymmetrical $\text{C}_\alpha=\text{C}_\beta$ stretching band, 1427 cm^{-1} assigned to symmetrical $\text{C}_\alpha=\text{C}_\beta(-\text{O})$ stretching band of thiophene ring, $\text{C}_\beta-\text{C}_\beta$ stretching band at 1368 cm^{-1} , 1258 cm^{-1} peak for $\text{C}_\alpha-\text{C}_{\alpha'}$ inter-ring stretching band and C-O-C deformation band with peak at 1097 cm^{-1} . The peak position and their assignments are in good agreement with reported intramolecular Raman vibration of PEDOT:PSS^{89,90}. Several studies^{53,91,92} have been focused on the effect of cosolvent and second dopant on PEDOT :PSS molecular structure and they observed red shift in Raman spectra of $\text{C}_\alpha=\text{C}_\beta$ stretching band ,(from ~

1440 to $\sim 1425 \text{ cm}^{-1}$), because of resonant structure transformation from benzoid to quinoid structure. While the benzoid structure has coil conformation and random orientation, the quinoid has linear or expanded-coil structure with filament shape PEDOT :PSS and higher charge carrier mobility. Upon over-oxidation reaction , C_{α} - C_{β} stretching band shifted to lower frequency compared to pristine PEDOT: PSS film (1427 to 1414 cm^{-1}). This shows quinoid structure is the predominant structure in over-oxidized PEDOT :PSS and although electrical conductivity decreases by PEDOT smearing, the PEDOT :PSS keeps its filament structure with PEDOT core and PSS shell. This open structure helps PEDOT: PSS chain to keep its ionic mobility while electronic conductance is reduced. Furthermore, the overall intensity of Raman spectra for over-oxidized polymer is higher than pristine film, indicating presence of excess PSS which are not anchored to PEDOT chain and they have been replaced by the oxidation process .

4-2-2 Effect of over-oxidation on PEDOT: PSS electronic structure change

UPS (Ultraviolet Photon Spectroscopy) has been used to study the electronic structure of pristine and over-oxidized PEDOT: PSS film. Polaron (radical-cation) and bipolarons (dication) are charge carriers in PEDOT: PSS conjugate polymer. By oxidizing the polymer, a cation-radical pair is formed and polymer structure changed from benzoid to quinoid in between the cation and the radical. This restrained change in bond order and its related charge is called polaron. If two electrons are withdrawn from PEDOT, a positive bipolaron is created. By oxidizing more, bipolaron energy bands and intra-chain in band gap will form in one dimension. The Fermi level lies in middle of the polaron band for polaronic polymer and between the valance and bipolaron band for bipolaronic polymer

^{93,94}. Analysis of UPS spectra near fermi level has been used to probe the energy levels. The UPS spectra of pristine and over-oxidized PEDOT :PSS in low energy region are shown in Figure 4-5-a.

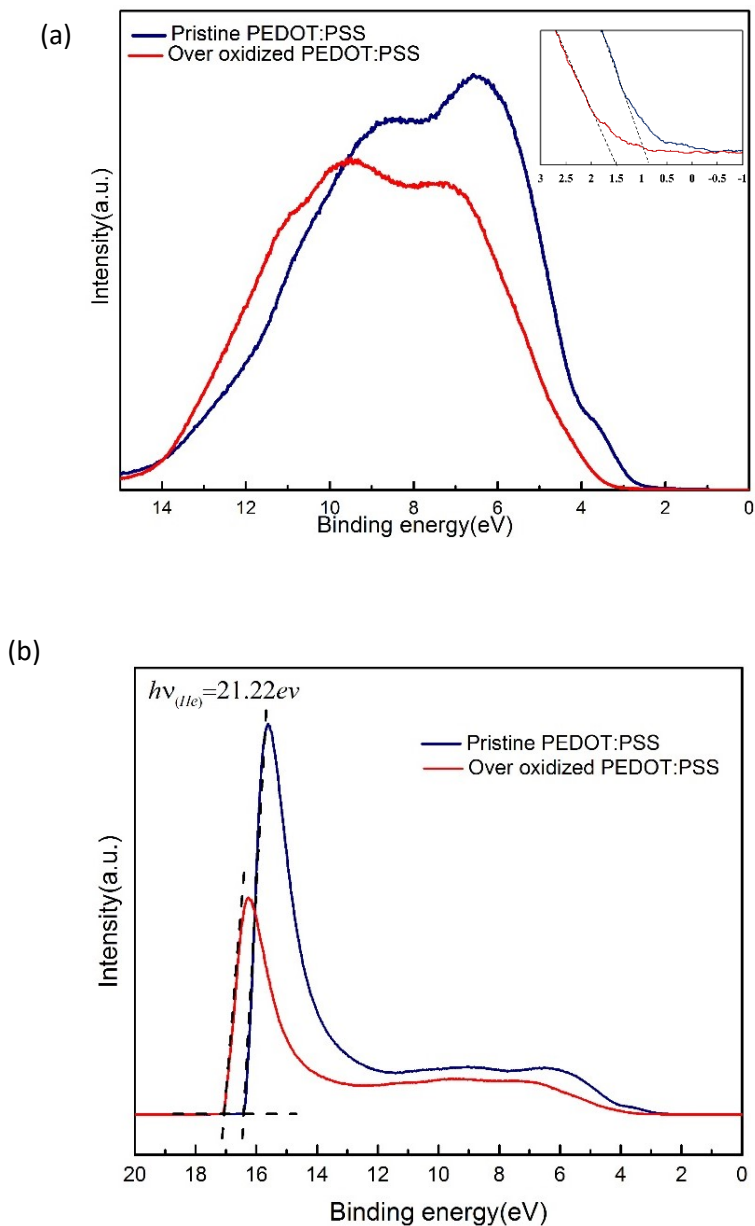


Fig 4-5 HOMO region of UPS spectrum for pristine and over-oxidized PEDOT :PSS (a) , UPS spectrum and cut off energy (b)

Figure 4-5 (a) inset has been used to measure the highest occupied molecular orbital (HOMO) value. UPS spectrum of PEDOT:PSS has a tail in low energies close to Fermi level (E_f). This is related to the localized filled states of disorderd polymer chain. Bubnova et.al⁹⁴ also reported similar spectrum for PEDOT:PSS. The pristine PEDOT:PSS spectrum shows a larger density of valence electronic state (DOVS) compared to over-oxidized film at E_f (higher intensity). Furthermore, HOMO for over-oxidized PEDOT:PSS (1.55eV compared to 0.8eV of pristine PEDOT: PSS) shifted away from the Fermi level to higher energies.

The UPS spectrum can also be used to determine the work function (Φ) of the sample using high binding energy cut off (HBEC) where $\Phi = h\nu - E_{\text{cutoff}}$. Fig 4-5-b compares the cut-off energy of two polymer film. Work function for pristine PEDOT:PSS (4.84 eV) is larger than work function of over-oxidized (4.16 eV) sample. However, ionization energy for both samples are not much different (5.74 eV for Pristine PEDOT: PSS compared to 5.71eV of over-oxidized PEDOT: PSS) and slight difference in ionization energy is because of structure change. Table 4-1 summarizes the energy level values for both pristine and over-oxidized sample.

Table4-1 energy level of pristine and oxidized PEDOT :PSS sample studied by UPS

<i>Sample</i>	<i>Work function (eV)</i>	<i>HOMO(eV)</i>	<i>Ionization Potential(eV)</i>
<i>Pristine PEDOT:PSS</i>	4.84	0.8	5.74
<i>Over-oxidized PEDOT: PSS</i>	4.16	1.55	5.71

Recent microscopy studies show that PEDOT: PSS has filament like structure. In these filaments, the core consists of hydrophobic PEDOT whereas the hydrophilic PSS forms the shell. Current transports through PEDOT rich regions along the filaments and charge hops inter filaments through the PSS region. The electrical conductivity is defined by charged carrier transport in PEDOT segment and their hopping between single or aggregated PEDOT regions along PSS chain^{95,96}. Upon over-oxidation, as the XPS data (figure 4-3) shows, some PEDOT segments degrade. This degradation disturbs polymer conjugation and decrease the amount of charge carriers and shifts the Fermi level further from valance band. Furthermore, the over-oxidation process shrinks the PEDOT region and increases charge hopping distance. Thus the decrease in the conduction is mainly due to the reaction of PEDOT with sodium hypochlorite which alters the charge transport intra and inter PEDOT chain. This happens due to reduction in the charged carriers, density of states near Fermi level and increase in the hopping distance. It is possible that through over-oxidation process, PSS dissolves partially in the oxidizing agent due to its hydrophilic nature. However, our XPS and Raman study shows PSS remains intact. Oostra et.al.⁸⁴ also observed significant change in electrical conduction without change in thickness of oxidized film.

The characteristics of pristine and over-oxidized PEDOT:PSS-based transistor were obtained by applying positive gate voltage for sweeping drain voltage and source -drain current was measured. Figure 4-6 (a-d) shows the output characteristics of an OECT based on pristine PEDOT: PSS and over-oxidized devices ($w=20\mu\text{m}$, $l=40\mu\text{m}$, $d=170\text{nm}$).

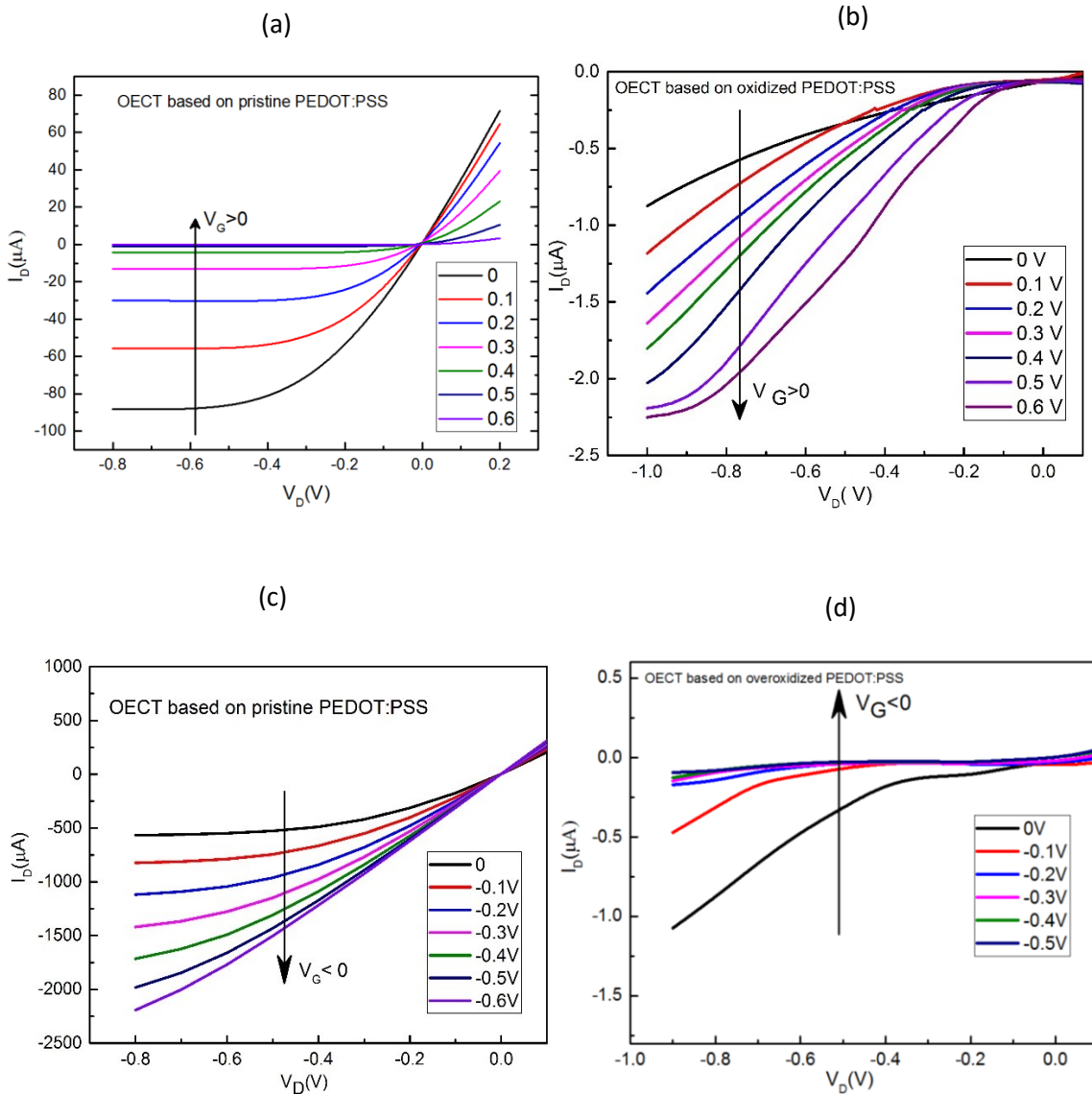


Figure 4-6 output characteristics of device upon applying positive gate voltage to OEECT based on pristine OEECT (a) and over oxidized PEDOT:PSS (b) and device characteristics upon application of negative gate voltage to OEECT based on Pristine (c) and over oxidized PEDOT :PSS (d)

Figure 4-6-a shows the device with typical characteristics of depletion mode transistor^{20,34} where unbiased channel is “ON” and by applying positive gate voltage device turns “OFF”. When positive bias is applied at gate, cations of electrolyte are injected into the

polymer and by compensating sulfonate anions on PSS dedope the channel and as a result absolute value of current decreases. This kind of OECTs was discussed in detail in Chapter three of the thesis.

While pristine PEDOT:PSS device operates in depletion mode, the over-oxidized PEDOT:PSS based transistor, functions in accumulation mode. Figure 4-6-b shows the characteristics of the over-oxidized PEDOT :PSS based device. By increasing positive gate voltage the current between source and drain increases, opposite of pristine PEDOT:PSS based transistor. As our PEDOT:PSS structure study shows, by over-oxidation reaction, PSS remains intact. PSS chain is hydrophilic and ion permeable. This property of PSS makes it possible for sodium cations to permeate into PSS structure when a positive bias is applied to the gate and the mobile ions will accumulate between source/drain. As a result the ionic conductivity occurs between two the electrodes. By increasing gate voltage, more cations will enter the PSS chain and ionic conductivity increases. It is rational to anticipate the reverse behavior by introducing an ions into the channel polymer. While anions (in this case Cl⁻) increases the doping and the hole concentration of the pristine PEDOT: PSS channel (figure 4-6-c), the anions create a depleted region of mobile ions and ionic conductivity decreases in OECT based on oxidized PEDOT: PSS. Berggren and his coworkers conduct the ionic selectivity of over-oxidized PEDOT :PSS to develop an ion pump ^{97,98}and ion bipolar junction transistor ^{99,100}. More I_D-V_D characteristics of OECTs based on pristine and over-oxidized PEDOT: PSS are presented in Appendix-B.

Transconductance, threshold voltage and ON/OFF current ratio has been studied with detail for depletion mode OECT in Chapter three of thesis. Here for comparison these

parameters are studied for OECT based on oxidized PEDOT :PSS. Figure 4-7 summarize device characteristics ($w=10\mu\text{m}$, $l=40\mu\text{m}$, $d=260\text{nm}$).

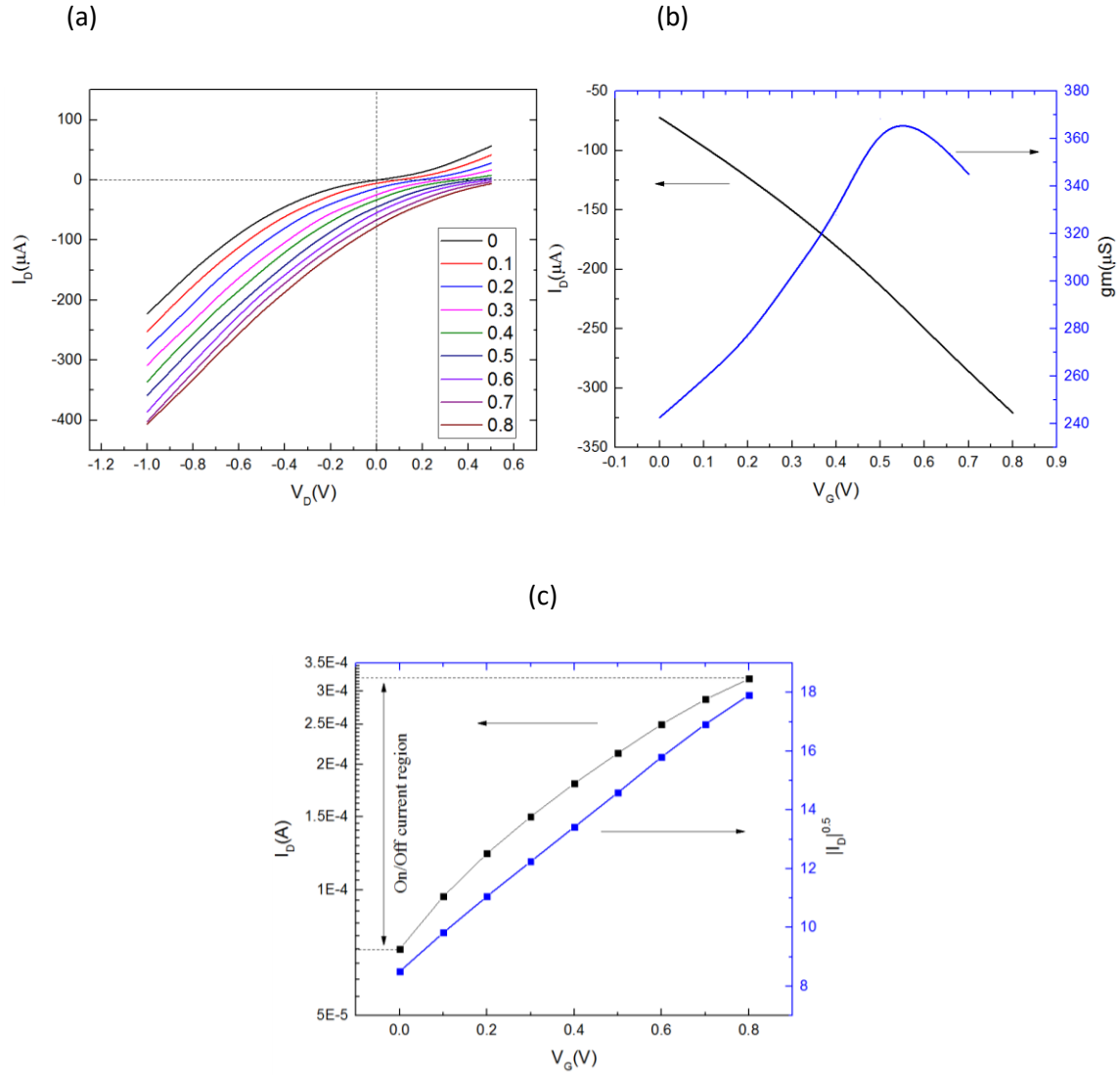


Figure 4-7 a) output characteristics of the device. V_G changing between 0 (bottom curve) to 0.8 V (top curve) b) transfer curve and OECT transconductance for V_D of -0.7v c) transfer characteristics with indication of ON/OFF current ratio for the device with oxidized PEDOT: PSS as channel ($w=10\mu\text{m}$, $l=40\mu\text{m}$, $d=260\text{nm}$)

Output characteristics of accumulation mode OECT shows an increase in current between source and drain by increasing gate voltage as explained for Figure 4-6(c-d). Figure 4-7 b shows the transconductance curve along with current transfer curve at -0.7V of drain voltage. as it is clear unlike depletion mode OECT, current increase by increasing gate voltage and transconductance reaches its maximum at higher gate voltage (0.6V) compared to depletion mode OECT. Furthermore, the ON/OFF ratio is poor (4.45) compared to depletion mode OECT. Whats more, the transfer curve shows that at gate voltages between 0-0.2V range there is still flow of current between source and drain at its OFF state and there is no clear threshold voltage.

4-3 Conclusion

PEDOT: PSS has a filament like structure in which current transports through PEDOT rich regions along the filaments and charge hops inter filaments through PSS region. Upon over oxidation, PEDOT segments degrade. This degradation, disturbs polymer conjugation and decrease the amount of charge carriers. Furthermore, the over-oxidation process shrinks the PEDOT region and increases the charge hopping distance. Although electrical conductivity is limited in over-oxidized PEDOT: PSS, the ionic conductivity which occurs primarily in the excess PSS remains intact. This property can be conducted to change the OECT device mode from depletion mode to accumulation mode.

5 Conclusion and future work

The purpose of this research is to better understand the mechanism of organic electrochemical transistor. This will help to design biosensors based on device properties and therefore maximize sensors sensitivity. To reach this aim, OECTs have been fabricated on flexible bio compatible Parylene substrate and its geometry studied as one potential sensor design parameter. Our results show that transconductance which is the change in current with change in applied gate voltage changes with w/l ratio of channel. There is linear relation between w/l ratio and device transconductance. For the devices with thickness of 260nm the transconductance changed from 592 μ S for w/l=0.4 to 1887 μ S for the device with w/l=2. This trend was observed for the devices with thickness of 170nm as well and transconductance changed from 42 μ S for w/l=0.4 to 217 μ S for the device with w/l=2 Also, it is been found that by changing width to length ratio one can reach maximum transconductance at low gate bias which makes sensors based on OECTs efficient. The study of channel thickness effect on device behavior shows that thinner devices(170nm compared to 260nm) have lower transconductance (217 μ S compared to 1887 μ S) and lower ON/OFF ratio (4.8×10^2 compared to 2.1×10^3) as well as lower threshold voltage (0.55V to 0.64V). Although the response time has not been studied here but it is anticipated to see faster response time on these devices. So it is crucial to use devices with optimum transconductance and speed. Preliminary capacitance studies, showed high specific capacitance (57 F/cm³) for our OECTs which is highest value reported for PEDOT: PSS based OECTs. However, this value is from single sample and might be higher than actual

capacitance because of ion accumulation on electrolyte/channel interface. High specific capacitance helps OECT to operate at low voltages and therefore they are good candidates in biosensing applications. High capacitance of PEDOT :PSS is because of its filament structure which lets charge carriers to hop through PEDOT regions and conducts electrical charge. Also, the amorphous PSS can hydrate and uptake ions from the channel. This structure leads to high hole mobility as well ($3.02 \text{ cm}^2/\text{V.s}$). The OECT model shows that in order to have device with high transconductance, the combination of mobility(μ) and transconductance(C^*) or the value of μC^* should be maximized by having optimum structure of PEDOT :PSS.

PEDOT: PSS has a filament like structure in which current transports through PEDOT rich regions along the filaments and charge hops inter filaments through PSS region. In this study, we investigate the effect of over-oxidation on PEDOT: PSS structure. XPS, UPS and Raman studies shows that the over-oxidation process shrinks the PEDOT region and increases the charge hopping distance. This structural change although it affects the electrical conductivity, the ionic conductivity which occurs primarily in the excess PSS remains intact. This property conducted to change the OECT device mode from depletion mode to accumulation mode all with one simple bleach oxidation treatment. The over-oxidized PPEDOT: PSS channel can be used as accumulation mode transistor next to depletion mode or to use as ionic sensor and even ion pump.

There a lot of ongoing research in designing sensors for the chemical measurements in brain that they are mostly based on microdialysis probe or in vivo electrochemical measurements. These devices are generally single terminal devices and the signal to noise

ratio is restricted by their size and therefore are highly invasive. OECTs have the potential to be used in brain's chemical study. So as a future work one can investigate the OECTs behavior as neurochemical sensor. Although OECTs can provide better platform for neurochemical sensing, yet they need to be designed to improve selectivity of sensors toward specific chemical. The main challenge in biosensor development is attaching bio receptors to the solid-state devices while maintaining their functionality. So as a future work, the designed OECTs can be functionalized with neuro receptor or ion pump to study the selectivity of OECT for different chemicals. Furthermore, as a device study, the OECTs performance can be studied by investigation of nanoparticle/ PEDOT: PSS to increase specific capacitance. Further study of crystal structure beside hole/ion mobility measurement on pristine and over-oxidized PEDOT: PSS also helps to understand the charge and ion transformation better.

Bibliography

1. Friend, R. H. *et al.* Electroluminescence in conjugated polymers. **397**, 121–128 (1999).
2. Lee, J. *et al.* Deep blue phosphorescent organic light-emitting diodes with very high brightness and efficiency. *Nat. Mater.* **15**, 92–8 (2016).
3. Grätzel, M. Photoelectrochemical cells. *Nature* **414**, 338–44 (2001).
4. Saliba, M. *et al.* A molecularly engineered hole-transporting material for efficient perovskite solar cells. *Nat. Energy* **1**, 15017 (2016).
5. Crone, B. *et al.* Large-scale complementary integrated circuits based on organic transistors. *Nature* **403**, 521–3 (2000).
6. Zang, Y. *et al.* Flexible suspended gate organic thin-film transistors for ultra-sensitive pressure detection. *Nat. Commun.* **6**, 6269 (2015).
7. Bubnova, O. *et al.* Optimization of the thermoelectric figure of merit in the conducting polymer poly(3,4-ethylenedioxythiophene). *Nat. Mater.* **10**, 429–33 (2011).
8. Du, Y. *et al.* Thermoelectric fabrics: toward power generating clothing. *Sci. Rep.* **5**, 6411 (2015).
9. Shirakawa, H., Louis, E. J., MacDiarmid, A. G., Chiang, C. K. & Heeger, A. J. Synthesis of electrically conducting organic polymers: halogen derivatives of polyacetylene, (CH). *J. Chem. Soc. Chem. Commun.* 578–580 (1977). doi:10.1039/C39770000578
10. Chiang, C. *et al.* Electrical Conductivity in Doped Polyacetylene. *Phys. Rev. Lett.* **39**, 1098–1101 (1977).
11. Kasap, S. O. *Principles of Electronic Materials and Devices*. (McGraw-Hill, 2006).
12. Atkins, P. & Paula, J. de. *Atkins' Physical Chemistry*. (OUP Oxford, 2010).
13. Sorrell, T. N. *Organic Chemistry*. (University Science Books, 2006).
14. Ouellette, R. J. & Rawn, J. D. *Organic Chemistry. Organic Chemistry* (Elsevier, 2014). doi:10.1016/B978-0-12-800780-8.00001-2
15. Hsieh, B. R. & Wei, Y. *Semiconducting polymers: applications, properties, and synthesis*. (American Chemical Society, 1999).
16. Georges Hadziioannou & Malliaras, G. G. *Semiconducting polymers: chemistry, physics and engineering*. (Wiley, 2007).

17. Zan, H. *Polymer Electronics*. **7**, (CRC Press, 1960).
18. So, F. *Organic Electronics: Materials, Processing, Devices and Applications*. *Organic Electronics* **8**, (CRC Press, 2010).
19. Elschner, A., Kirchmeyer, S., Lovenich, W., Merker, U. & Reuter, K. *PEDOT: Principles and Applications of an Intrinsically Conductive Polymer*. **2**, (CRC Press, 2010).
20. Khodagholy, D. *et al.* High transconductance organic electrochemical transistors. *Nat. Commun.* **4**, 2133 (2013).
21. Koezuka, H., Tsumura, A. & Ando, T. Field-effect transistor with polythiophene thin film. *Synth. Met.* **18**, 699–704 (1987).
22. Woll, C. *Physical and Chemical Aspects of Organic Electronics*. (John Wiley & Sons, 2009).
23. Du, H., Lin, X., Xu, Z. & Chu, D. Electric double-layer transistors: a review of recent progress. *J. Mater. Sci.* **50**, 5641–5673 (2015).
24. He, X., Liu, F., Zeng, Q. & Liu, Z. Electric-double-layer Transistors Based on Two Dimensional Materials. *Acta Chim. Sin.* **73**, 924 (2015).
25. Lee, S.-K. *et al.* Stretchable graphene transistors with printed dielectrics and gate electrodes. *Nano Lett.* **11**, 4642–6 (2011).
26. Cho, J. H. *et al.* Printable ion-gel gate dielectrics for low-voltage polymer thin-film transistors on plastic. *Nat. Mater.* **7**, 900–6 (2008).
27. Ozel, T., Gaur, A., Rogers, J. A. & Shim, M. Polymer electrolyte gating of carbon nanotube network transistors. *Nano Lett.* **5**, 905–11 (2005).
28. Lin, M.-W. *et al.* Mobility enhancement and highly efficient gating of monolayer MoS₂ transistors with polymer electrolyte. *J. Phys. D: Appl. Phys.* **45**, 345102 (2012).
29. Sun, M., Lan, L., Wang, L., Peng, J. & Cao, Y. Synthesis of Novel Conjugated Polyelectrolytes for Organic Field-Effect Transistors Gate Dielectric Materials. *Macromol. Chem. Phys.* **209**, 2504–2509 (2008).
30. Dankerl, M., Tosun, M., Stutzmann, M. & Garrido, J. A. Solid polyelectrolyte-gated surface conductive diamond field effect transistors. *Appl. Phys. Lett.* **100**, 023510 (2012).
31. Kergoat, L., Piro, B., Berggren, M., Horowitz, G. & Pham, M.-C. Advances in organic transistor-based biosensors: from organic electrochemical transistors to electrolyte-gated organic field-effect transistors. *Anal. Bioanal. Chem.* **402**, 1813–26 (2012).
32. Kim, S. H. *et al.* Electrolyte-gated transistors for organic and printed electronics. *Adv. Mater.* **25**, 1822–46 (2013).

33. White, H. S., Kittlesen, G. P. & Wrighton, M. S. Chemical derivatization of an array of three gold microelectrodes with polypyrrole: fabrication of a molecule-based transistor. *J. Am. Chem. Soc.* **106**, 5375–5377 (1984).
34. Rivnay, J. *et al.* Organic electrochemical transistors with maximum transconductance at zero gate bias. *Adv. Mater.* **25**, 7010–4 (2013).
35. Bernardis, D. A. & Malliaras, G. G. Steady-State and Transient Behavior of Organic Electrochemical Transistors. *Adv. Funct. Mater.* **17**, 3538–3544 (2007).
36. Sessolo, M. *et al.* Easy-to-fabricate conducting polymer microelectrode arrays. *Adv. Mater.* **25**, 2135–9 (2013).
37. Kumar, A. & Sinha, J. *Organic Semiconductors in Sensor Applications*. **107**, (Springer Berlin Heidelberg, 2008).
38. Strakosas, X., Bongo, M. & Owens, R. M. The organic electrochemical transistor for biological applications. *J. Appl. Polym. Sci.* **132**, n/a–n/a (2015).
39. Lin, P. & Yan, F. Organic thin-film transistors for chemical and biological sensing. *Adv. Mater.* **24**, 34–51 (2012).
40. Tarabella, G. *et al.* Liposome sensing and monitoring by organic electrochemical transistors integrated in microfluidics. *Biochim. Biophys. Acta* **1830**, 4374–80 (2013).
41. Tarabella, G. *et al.* Organic electrochemical transistors monitoring micelle formation. *Chem. Sci.* **3**, 3432 (2012).
42. Sessolo, M., Rivnay, J., Bandiello, E., Malliaras, G. G. & Bolink, H. J. Ion-selective organic electrochemical transistors. *Adv. Mater.* **26**, 4803–7 (2014).
43. Mousavi, Z., Ekholm, A., Bobacka, J. & Ivaska, A. Ion-Selective Organic Electrochemical Junction Transistors Based on Poly(3,4-ethylenedioxythiophene) Doped with Poly(styrene sulfonate). *Electroanalysis* **21**, 472–479 (2009).
44. Liao, C., Zhang, M., Niu, L., Zheng, Z. & Yan, F. Highly selective and sensitive glucose sensors based on organic electrochemical transistors with graphene-modified gate electrodes. *J. Mater. Chem. B* **1**, 3820 (2013).
45. Liao, C., Mak, C., Zhang, M., Chan, H. L. W. & Yan, F. Flexible organic electrochemical transistors for highly selective enzyme biosensors and used for saliva testing. *Adv. Mater.* **27**, 676–81 (2015).
46. Khodagholy, D. *et al.* Organic electrochemical transistor incorporating an ionogel as a solid state electrolyte for lactate sensing. *J. Mater. Chem.* **22**, 4440 (2012).
47. He, R.-X. *et al.* Detection of bacteria with organic electrochemical transistors. *J. Mater. Chem.* **22**, 22072 (2012).
48. Lin, P., Luo, X., Hsing, I.-M. & Yan, F. Organic electrochemical transistors integrated in flexible microfluidic systems and used for label-free DNA sensing.

- Adv. Mater.* **23**, 4035–40 (2011).
49. Campana, A., Cramer, T., Simon, D. T., Berggren, M. & Biscarini, F. Electrocardiographic recording with conformable organic electrochemical transistor fabricated on resorbable bioscaffold. *Adv. Mater.* **26**, 3874–8 (2014).
 50. Khodagholy, D. *et al.* In vivo recordings of brain activity using organic transistors. *Nat. Commun.* **4**, 1575 (2013).
 51. Kumatani, A., Li, Y., Darmawan, P., Minari, T. & Tsukagoshi, K. On practical charge injection at the metal/organic semiconductor interface. *Sci. Rep.* **3**, 1026 (2013).
 52. Jönsson, S. K. *et al.* The effects of solvents on the morphology and sheet resistance in poly(3,4-ethylenedioxythiophene)–polystyrenesulfonic acid (PEDOT–PSS) films. *Synth. Met.* **139**, 1–10 (2003).
 53. Ouyang, J. *et al.* On the mechanism of conductivity enhancement in poly(3,4-ethylenedioxythiophene):poly(styrene sulfonate) film through solvent treatment. *Polymer (Guildf)*. **45**, 8443–8450 (2004).
 54. Mukherjee, A. K., Thakur, A. K., Takashima, W. & Kaneto, K. Minimization of contact resistance between metal and polymer by surface doping. *J. Phys. D. Appl. Phys.* **40**, 1789–1793 (2007).
 55. Stavrinidou, E. *et al.* Direct measurement of ion mobility in a conducting polymer. *Adv. Mater.* **25**, 4488–93 (2013).
 56. Taylor, P. G. *et al.* Orthogonal Patterning of PEDOT:PSS for Organic Electronics using Hydrofluoroether Solvents. *Adv. Mater.* **21**, 2314–2317 (2009).
 57. Orthogonal solvents and compatible photoresists for the photolithographic patterning of organic electronic devices. (2014).
 58. Schwartz, E. L., Chan, W. M., Lee, J. K., Tiwari, S. & Ober, C. K. Methods of making patterned structures of materials, patterned structures of materials, and methods of using same. (2014).
 59. Prigodin, V. N. *et al.* Electric Field Control of Charge Transport in Doped Polymers. *Synth. Met.* **153**, 157–160 (2005).
 60. Tu, D., Kergoat, L., Crispin, X., Berggren, M. & Forchheimer, R. Transient analysis of electrolyte-gated organic field-effect transistors. in *SPIE Organic Photonics + Electronics* (eds. Bao, Z. & McCulloch, I.) 84780L (International Society for Optics and Photonics, 2012). doi:10.1117/12.929886
 61. Coppedè, N., Villani, M. & Gentile, F. Diffusion driven selectivity in organic electrochemical transistors. *Sci. Rep.* **4**, 4297 (2014).
 62. Friedlein, J. T., Shaheen, S. E., Malliaras, G. G. & McLeod, R. R. Optical Measurements Revealing Nonuniform Hole Mobility in Organic Electrochemical

- Transistors. *Adv. Electron. Mater.* **1**, n/a–n/a (2015).
63. Pettersson, L. A. ., Ghosh, S. & Inganäs, O. Optical anisotropy in thin films of poly(3,4-ethylenedioxythiophene)–poly(4-styrenesulfonate). *Org. Electron.* **3**, 143–148 (2002).
 64. Gasiorowski, J., Menon, R., Hingerl, K., Dachev, M. & Sariciftci, N. S. Surface morphology, optical properties and conductivity changes of poly(3,4-ethylenedioxythiophene):poly(styrenesulfonate) by using additives. *Thin Solid Films* **536**, 211–215 (2013).
 65. Nardes, A. M. *et al.* Microscopic Understanding of the Anisotropic Conductivity of PEDOT:PSS Thin Films. *Adv. Mater.* **19**, 1196–1200 (2007).
 66. van de Ruit, K. *et al.* The Curious Out-of-Plane Conductivity of PEDOT:PSS. *Adv. Funct. Mater.* **23**, 5787–5793 (2013).
 67. Okuzaki, H., Harashina, Y. & Yan, H. Highly conductive PEDOT/PSS microfibers fabricated by wet-spinning and dip-treatment in ethylene glycol. *Eur. Polym. J.* **45**, 256–261 (2009).
 68. Kim, Y. H. *et al.* Highly Conductive PEDOT:PSS Electrode with Optimized Solvent and Thermal Post-Treatment for ITO-Free Organic Solar Cells. *Adv. Funct. Mater.* **21**, 1076–1081 (2011).
 69. Fan, B., Mei, X. & Ouyang, J. Significant Conductivity Enhancement of Conductive Poly(3,4-ethylenedioxythiophene):Poly(styrenesulfonate) Films by Adding Anionic Surfactants into Polymer Solution. *Macromolecules* **41**, 5971–5973 (2008).
 70. Alemu, D., Wei, H.-Y., Ho, K.-C. & Chu, C.-W. Highly conductive PEDOT:PSS electrode by simple film treatment with methanol for ITO-free polymer solar cells. *Energy Environ. Sci.* **5**, 9662 (2012).
 71. Hütter, P. C., Rothländer, T., Haase, A., Trimmel, G. & Stadlober, B. Influence of geometry variations on the response of organic electrochemical transistors. *Appl. Phys. Lett.* **103**, 043308 (2013).
 72. Rivnay, J. *et al.* High-performance transistors for bioelectronics through tuning of channel thickness. *Sci. Adv.* **1**, e1400251 (2015).
 73. Xu, H. *et al.* Top-gated graphene field-effect transistors with high normalized transconductance and designable dirac point voltage. *ACS Nano* **5**, 5031–7 (2011).
 74. Schamoni, H., Noever, S., Nickel, B., Stutzmann, M. & Garrido, J. A. α,ω -dihexylsexithiophene thin films for solution-gated organic field-effect transistors. *Appl. Phys. Lett.* **108**, 073301 (2016).
 75. Wang, C. *et al.* Significance of the double-layer capacitor effect in polar rubbery dielectrics and exceptionally stable low-voltage high transconductance organic transistors. *Sci. Rep.* **5**, 17849 (2015).

76. Kumar, P. *et al.* Effect of channel thickness, electrolyte ions, and dissolved oxygen on the performance of organic electrochemical transistors. *Appl. Phys. Lett.* **107**, 053303 (2015).
77. Yoo, D. *et al.* Gradual thickness-dependent enhancement of the thermoelectric properties of PEDOT:PSS nanofilms. *RSC Adv.* **4**, 58924–58929 (2014).
78. Chiang, C.-H. & Wu, C.-G. High-efficient dye-sensitized solar cell based on highly conducting and thermally stable PEDOT:PSS/glass counter electrode. *Org. Electron.* **14**, 1769–1776 (2013).
79. Takano, T., Masunaga, H., Fujiwara, A., Okuzaki, H. & Sasaki, T. PEDOT Nanocrystal in Highly Conductive PEDOT:PSS Polymer Films. *Macromolecules* **45**, 3859–3865 (2012).
80. Friedel, B. *et al.* Effects of Layer Thickness and Annealing of PEDOT:PSS Layers in Organic Photodetectors. (2009). doi:10.1021/ma901182u
81. Proctor, C. M., Rivnay, J. & Malliaras, G. G. Understanding volumetric capacitance in conducting polymers. *J. Polym. Sci. Part B Polym. Phys.* n/a–n/a (2016). doi:10.1002/polb.24038
82. Heeger, A. J. Semiconducting and Metallic Polymers: The Fourth Generation of Polymeric Materials (Nobel Lecture) Copyright(c) The Nobel Foundation 2001. We thank the Nobel Foundation, Stockholm, for permission to print this lecture. *Angew. Chem. Int. Ed. Engl.* **40**, 2591–2611 (2001).
83. TEHRANI, P. *et al.* The effect of pH on the electrochemical over-oxidation in PEDOT:PSS films. *Solid State Ionics* **177**, 3521–3527 (2007).
84. Oostra, A. J., van den Bos, K. H. W., Blom, P. W. M. & Michels, J. J. Disruption of the electrical conductivity of highly conductive poly(3,4-ethylenedioxythiophene):poly(styrene sulfonate) by hypochlorite. *J. Phys. Chem. B* **117**, 10929–35 (2013).
85. Rani, V. & Santhanam, K. S. V. Polycarbazole-based electrochemical transistor. *J. Solid State Electrochem.* **2**, 99–101 (1998).
86. Thackeray, J. W., White, H. S. & Wrighton, M. S. Poly(3-methylthiophene)-coated electrodes: optical and electrical properties as a function of redox potential and amplification of electrical and chemical signals using poly(3-methylthiophene)-based microelectrochemical transistors. *J. Phys. Chem.* **89**, 5133–5140 (1985).
87. Paul, E. W., Ricco, A. J. & Wrighton, M. S. Resistance of polyaniline films as a function of electrochemical potential and the fabrication of polyaniline-based microelectronic devices. *J. Phys. Chem.* **89**, 1441–1447 (1985).
88. Greczynski, G., Kugler, T. & Salaneck, W. . Characterization of the PEDOT-PSS system by means of X-ray and ultraviolet photoelectron spectroscopy. *Thin Solid Films* **354**, 129–135 (1999).

89. Farah, A. A. *et al.* Conductivity enhancement of poly(3,4-ethylenedioxythiophene)-poly(styrenesulfonate) films post-spincoating. *J. Appl. Phys.* **112**, 113709 (2012).
90. Garreau, S., Louarn, G., Buisson, J. P., Froyer, G. & Lefrant, S. In Situ Spectroelectrochemical Raman Studies of Poly(3,4-ethylenedioxythiophene) (PEDT). *Macromolecules* **32**, 6807–6812 (1999).
91. Ouyang, J., Chu, C., Chen, F., Xu, Q. & Yang, Y. Polymer Optoelectronic Devices with High-Conductivity Poly(3,4-Ethylenedioxythiophene) Anodes. *J. Macromol. Sci. Part A* **41**, 1497–1511 (2004).
92. Thomas, J. P. *et al.* Reversible structural transformation and enhanced performance of PEDOT:PSS-based hybrid solar cells driven by light intensity. *ACS Appl. Mater. Interfaces* **7**, 7466–70 (2015).
93. Braun, S., Salaneck, W. R. & Fahlman, M. Energy-Level Alignment at Organic/Metal and Organic/Organic Interfaces. *Adv. Mater.* **21**, 1450–1472 (2009).
94. Bubnova, O. *et al.* Semi-metallic polymers. *Nat. Mater.* **13**, 190–4 (2014).
95. VITORATOS, E. *et al.* Thermal degradation mechanisms of PEDOT:PSS. *Org. Electron.* **10**, 61–66 (2009).
96. van de Ruit, K. *et al.* Quasi-One Dimensional in-Plane Conductivity in Filamentary Films of PEDOT:PSS. *Adv. Funct. Mater.* **23**, 5778–5786 (2013).
97. Isaksson, J. *et al.* Electronic control of Ca²⁺ signalling in neuronal cells using an organic electronic ion pump. *Nat. Mater.* **6**, 673–9 (2007).
98. Jonsson, A. *et al.* Therapy using implanted organic bioelectronics. *Sci. Adv.* **1**, e1500039–e1500039 (2015).
99. Tybrandt, K., Larsson, K. C., Richter-Dahlfors, A. & Berggren, M. Ion bipolar junction transistors. *Proc. Natl. Acad. Sci. U. S. A.* **107**, 9929–32 (2010).
100. Tybrandt, K., Forchheimer, R. & Berggren, M. Logic gates based on ion transistors. *Nat. Commun.* **3**, 871 (2012).

Appendix A

Section A-1 is the step by step procedure of OECT fabrication and the recipe of photoresist used in fabrication process. In section A-2, the fabrication step of OECT based on sacrificial layer of Parylene is presented.

A-1 OECT fabrication steps

1-Parylene C Deposition on Si substrate

- Parylene amount: 5.5gr
- Parylene thickness: 3 μm



2- Photolithography for pads and contacts patterning

- Photoresist: AZ 5214
- Parameters:
 - Spread at 500 rpm for 10 Sec
 - Spin at 4000 rpm for 45 Sec
 - Soft bake 1 min at 90 °C
 - Expose 9 Sec
 - Second bake:40 Sec at 110 °C
 - Flood expose 1 min
 - Develop in MF 319 for 20 Sec



3-Source/drain/ wires/pads deposition and Ti/Au lift off

- Source/drain/ wires and pads are all Au. Ti has been used as an adhesive.

- BOB sputtering tool has been used for deposition. The Ti/Au deposition time was 2/15 min with approximate rate of the rate is 5.7nm/min for Ti and 6.87nm.min for Au.
- Acetone has been used for lift off

4-Parylene C Deposition on Si substrate

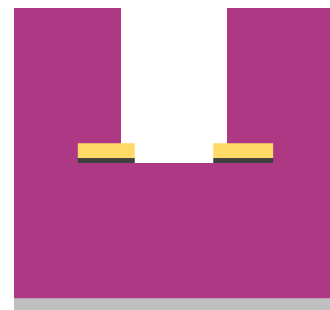
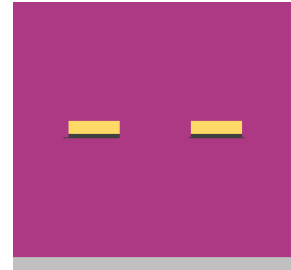
Same as step 1.

5-Channel and gate opening lithography

- Photoresist: HPR 506
- Parameters:
 - Spread at 500 rpm for 10 Sec
 - Spin at 2000 rpm for 40 Sec
 - Soft bake 90 sec at 115 °C
 - Rehydrate 15 min
 - Expose 13.5 Sec
 - Develop in 354 for 25 Sec
 - Hard bake 90 sec at 90 °C

6- Channel and gate opening

- micro etch RIE has been used for Parylene etching.
- Parameters:
 - Gas: Oxygen
 - Flow: 100%



Pressure: 150 mT

Power: 100 W

Time: 18 min

7-PEDOT: PSS patterning

- After PEDOT: PSS spin coating the unwanted PEDOT: PSS area has been deactivated. Acid sensitive photoresists are affected by acidic PEDOT: PSS and PEDOT: PSS films are damaged by standard developers. So I used fluorinated orthogonal OSCoR negative photoresist. The resist is research resist and it last for less than one year.

- Parameters:

Spread at 500 rpm for 10 Sec

Spin at 1000 rpm for 60 Sec

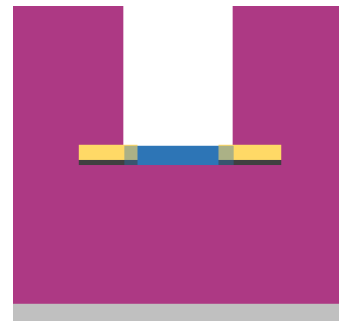
Soft bake 60 sec at 90 °C

Expose 4 Sec

Post bake 60 sec at 90 °C

Develop 90 Sec.

- To deactivate the unwanted PEDOT: PSS area Clorox bleach has been used for 15 Sec and resist striped by striping agent.



A-2 OECT fabrication based on sacrificial layer of Parylene

Step a-c of fabrication process is similar to the other technique which has been used to fabricated all OECTs in this thesis. However, as sacrificial technique is the common

fabrication process for the patterning of PEDOT: PSS in the literature it has been tested initially. Fabrication started by Parylene C deposition(a). Gold as source, drain, connection pad and conductive wires patterned using lift off lithography process(b) and another layer of Parylene insulate the connections(c). A, layer of soap (micro 90) used as anti- adhesive layer for peeling the sacrificial layer of Parylene and sacrificial Parylene deposited (d). The channel area defined by second step of lithography (HPR 506 as resist) and parylene etched by RIE (O2 plasma). After PEDOT: PSS spun coating (e), the sacrificial Parylene has been removed (f).

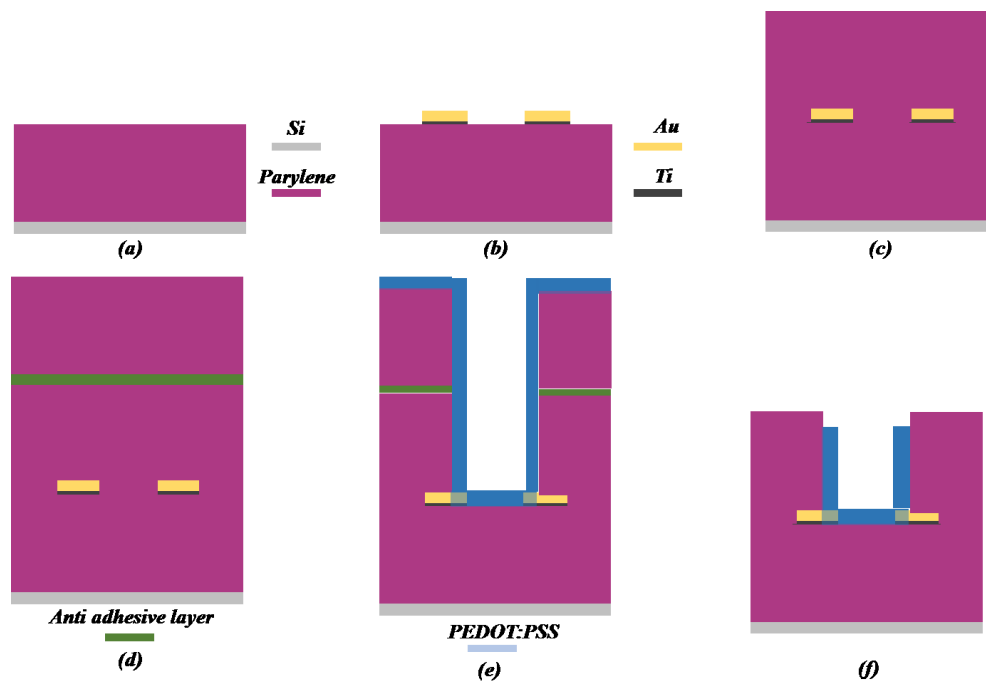


Fig A- 1) Parylene deposition (a) Source, drain and contact pad deposition (b) Parylene deposition to insulate electrodes(c) Sacrificial parylene deposition (d) channel and gate opening (RIE) and PEDOT: PSS coating (e) Sacrificial layer removing and PEDOT: PSS baking (f)

Figure A-2 shows the optical microscope image of OECTs fabricated by this technique. The issues with this method was bubble formation due to the soap, PEDOT: PSS peeling while removing sacrificial layer and poor electrical contact due to the remaining soap. So for the rest of research the OECTs fabricated by patterning PEDOT: PSS using HFE photoresist.

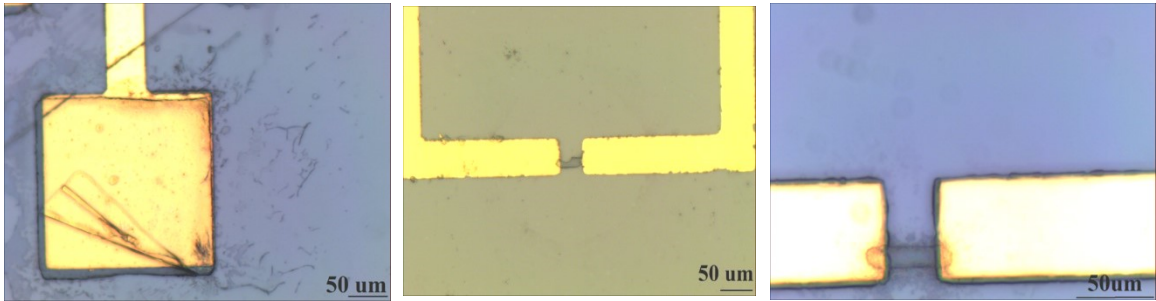


Figure A-2 Optical microscope image of OECTs fabricated by sacrificial layer of Parylene

Appendix B

The characteristics of pristine and over-oxidized PEDOT:PSS-based transistor were obtained by applying positive gate voltage for sweeping drain voltage and source -drain current was measured. Figure B-1 to B-3 show the output characteristics of an OECT based on pristine PEDOT:PSS and over-oxidized devices. The OECTs based on pristine PEDOT:PSS show depletion mode behavior and the OECTs based on over-oxidized PEDOT:PSS show accumulation mode behavior.

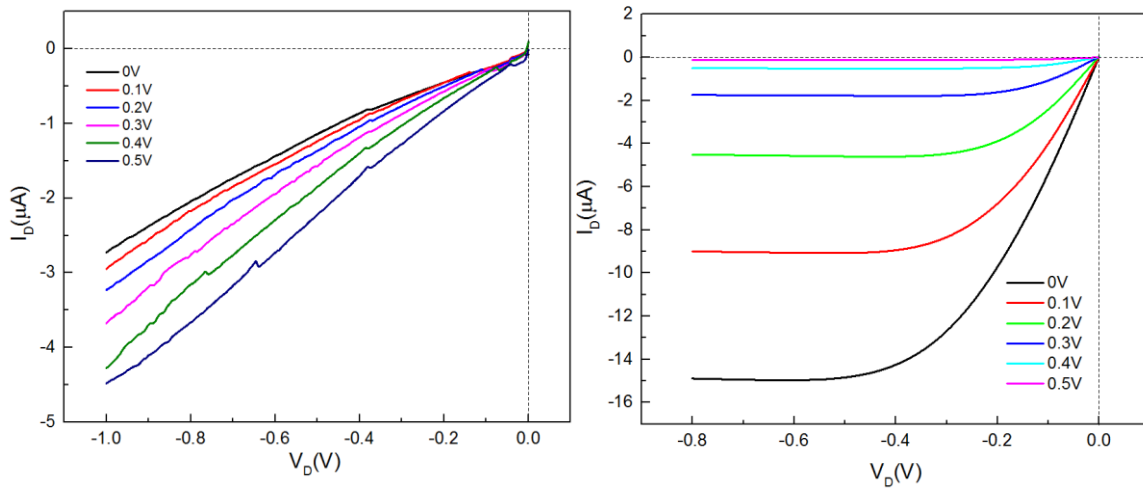


Figure B-1-output characteristics of the device with dimensions of $w=20\mu\text{m}$, $l=50\mu\text{m}$ and $d=170\text{nm}$. V_G changing between 0 to 0.5 V (right OECT based on pristine PEDOT:PSS and depletion mode device and left OECT based on over-oxidized PEDOT:PSS and accumulation device)

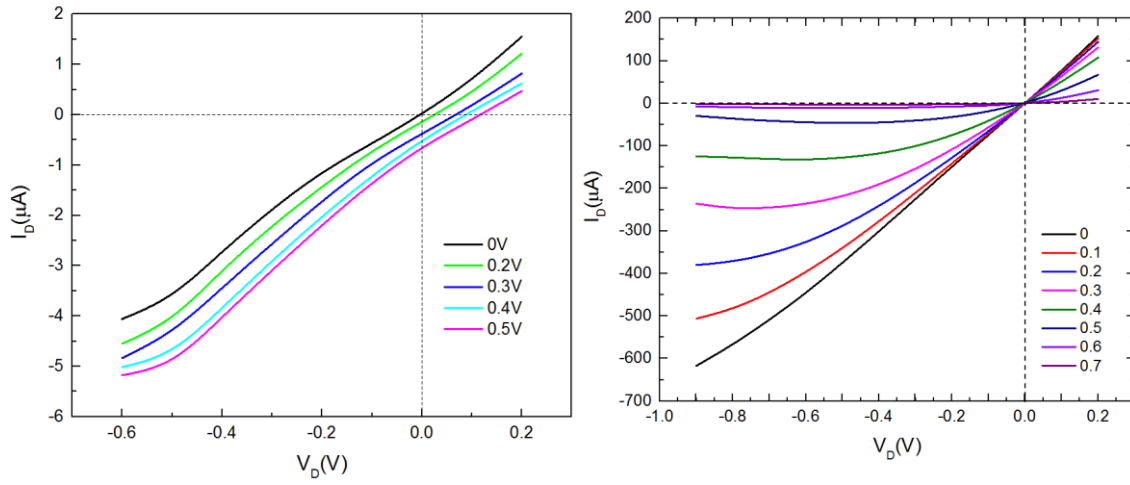


Figure B-2 output characteristics of the device with dimensions of $w=20\mu\text{m}$, $l=40\mu\text{m}$ and $d=260\text{nm}$. (right OECT based on pristine PEDOT: PSS and depletion mode device and left OECT based on over-oxidized PEDOT: PSS and accumulation device)

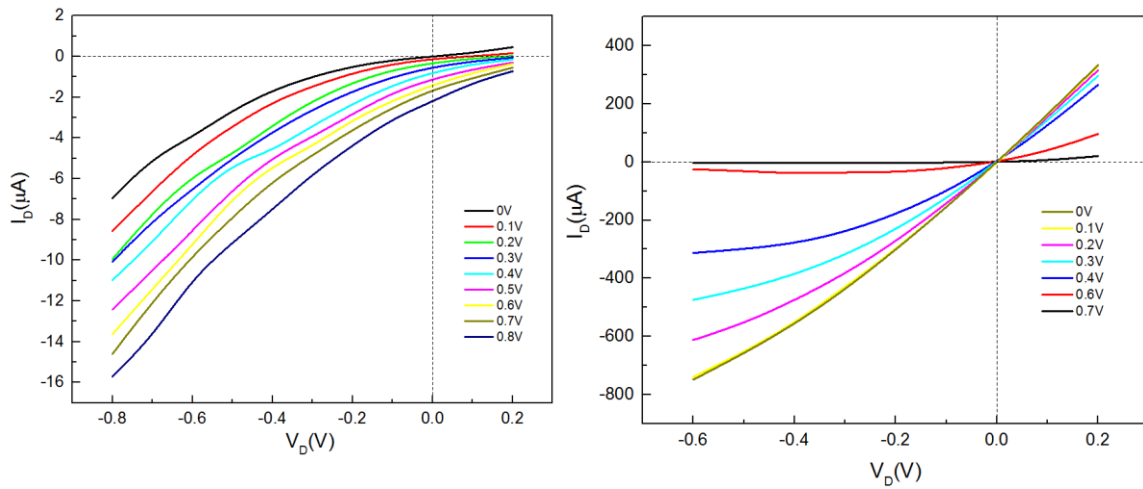


Figure B-3 output characteristics of the device with dimensions of $w=20\mu\text{m}$, $l=5\mu\text{m}$ and $d=260\text{nm}$. (right OECT based on pristine PEDOT: PSS and depletion mode device and left OECT based on over-oxidized PEDOT: PSS and accumulation device)